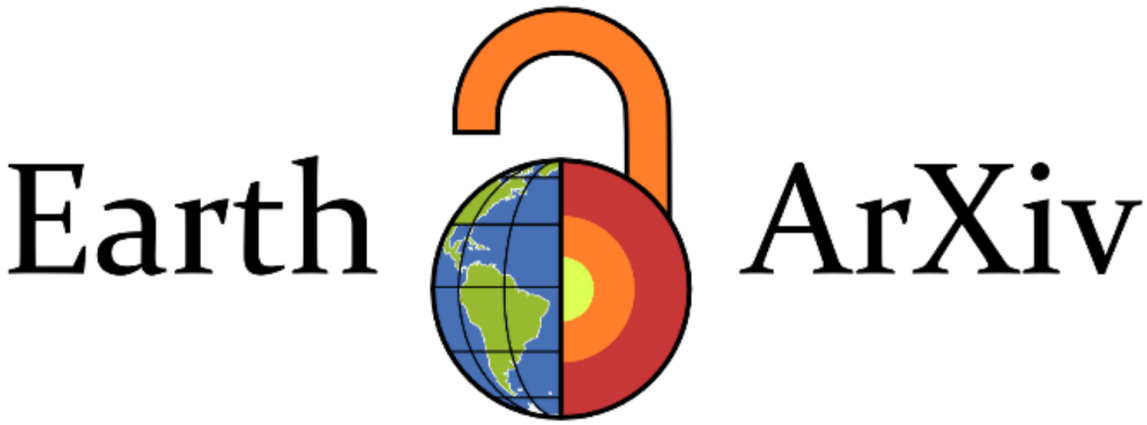

Peer review status: This is a non-peer-reviewed preprint submitted to EarthArXiv

Title: Local heat islands and vegetation losses are microclimatic consequences of global data centers

Authors: TC Chakraborty*

Affiliations: Pacific Northwest National Laboratory, Richland, WA, USA

*Corresponding author: TC Chakraborty (tc.chakraborty@pnnl.gov)

Classification: Physical Sciences/Earth, Atmospheric, and Planetary Sciences

Abstract The explosion in cloud computing and artificial intelligence has driven a rapid expansion of data centers. While the immense energy and water consumption of these facilities is well-documented, their impacts on local microclimates remain largely unexplored. Here, using satellite-derived estimates of land surface temperature and surface greenness, we isolate the microclimate footprint of almost 10,000 data centers globally. Our findings demonstrate a clear data center heat island effect (summer mean of 1.44 °C) accompanied and primarily modulated by localized vegetation reductions. Furthermore, near-term projections of human population growth in proximity to these facilities reveal the scale of their direct and indirect human impacts. These results underscore that data centers cause local environmental modification, necessitating integrated spatial planning to mitigate impacts on surrounding communities.

Main Text

The modern global economy has become increasingly tethered to data center infrastructure (*1*). Driven by the accelerated adoption of cloud computing, blockchain technologies, and, most recently, artificial intelligence (AI), the demand for data processing and storage has surged. To meet this demand, data centers, including massive hyperscale facilities, have proliferated across the globe. Historically, environmental impact assessments of these facilities have predominantly focused on their resource consumption, specifically, their substantial electricity requirements, subsequent greenhouse gas emissions, and the large volumes of water required for cooling systems (*2*–*6*). However, a critical dimension of their environmental footprint has been largely overlooked: the direct alteration of local land cover, the resulting modulation of surface microclimates, and the potential for concurrent human impacts due to these localized shifts (*7*, *8*).

The construction of large-scale data centers constitutes a distinct and intensive form of land use and land cover change (LULCC) (*9*). Physically, these facilities are characterized by vast, highly contiguous expanses of impervious surfaces, including sprawling building roofs, extensive parking lots, and supporting utility infrastructure. Converting natural or agricultural land to heavy industrial use reduces the local evaporative fraction by removing vegetation (*8*). Unlike typical commercial or residential infrastructure, data centers must continuously dissipate massive anthropogenic waste heat to prevent server throttling. This continuous thermal emission, combined with the high thermal inertia of their construction materials, can theoretically cause localized alteration of the surface energy balance.

While the Urban Heat Island (UHI) effect (*10*), whereby built environments exhibit significantly higher temperatures than their rural surroundings, is a well-established phenomenon, traditional UHI research primarily examines aggregations of residential, commercial, and mixed-use urban landscapes. Data centers have been argued to be a novel built typology (*9*, *11*). They are hyper-concentrated nodes of continuous thermal emission, often strategically situated on the peripheries of existing urban centers to capitalize on cheaper land and direct access to power grids and municipal water suppliers (*6*, *8*). Consequently, the introduction of a data center can act as a localized thermal perturbation to a landscape, generating an intense, highly localized heat island that may differ mechanistically from gradual, broad-scale urbanization.

Despite the rapid scaling of this digital footprint, there is a notable gap in systematic, global quantification regarding how the physical presence of data centers drives localized warming, vegetation degradation, and the implications of these changes for population-level impacts (*7*, *12*, *13*). Previous approaches to estimating large-scale historical climate change or LULCC impacts (*14*) either ignore these isolated industrial footprints entirely or group them within broader "urban" classifications in models and observations, thereby obscuring their unique signatures. Currently, only a single local-scale analysis (*12*) has shown empirical evidence of local thermal hazard modifications due to data centers.

Here, we provide a global, high-resolution assessment of the local microclimatic and ecological impacts of data centers. Leveraging a comprehensive spatial database of over 10,000 global facilities (*15*), we fuse thousands of satellite images and several satellite-derived datasets to isolate their specific environmental signals from broader regional climatology. We find that data centers often generate a distinct heat island effect, being warmer than their immediate surroundings. This warming is driven by the highly localized vegetation degradation due to data center construction, with no significant impact found of their unique thermal emissions at these scales, at least for satellite-derived Land Surface Temperature (LST). Furthermore, our demographic analysis reveals substantial and rapidly growing human populations directly around these facilities. Ultimately, these findings demonstrate localized environmental and human costs of the digital age, highlighting the pressing need for integrated sustainable planning in future cloud and AI infrastructure development.

Global distribution of and demographic proximity to data centers

To quantify the physical and human footprint of the digital age, we first analyzed a comprehensive, high-resolution spatial database (*15*) of 12,639 global data centers (Fig. 1A). Of these, 10,296 were built before 2025. The geographic distribution of these facilities exhibits clear spatial clustering, with the majority of these facilities concentrated across North America, Western Europe, and rapidly developing technological hubs in East Asia (Fig. 1B).

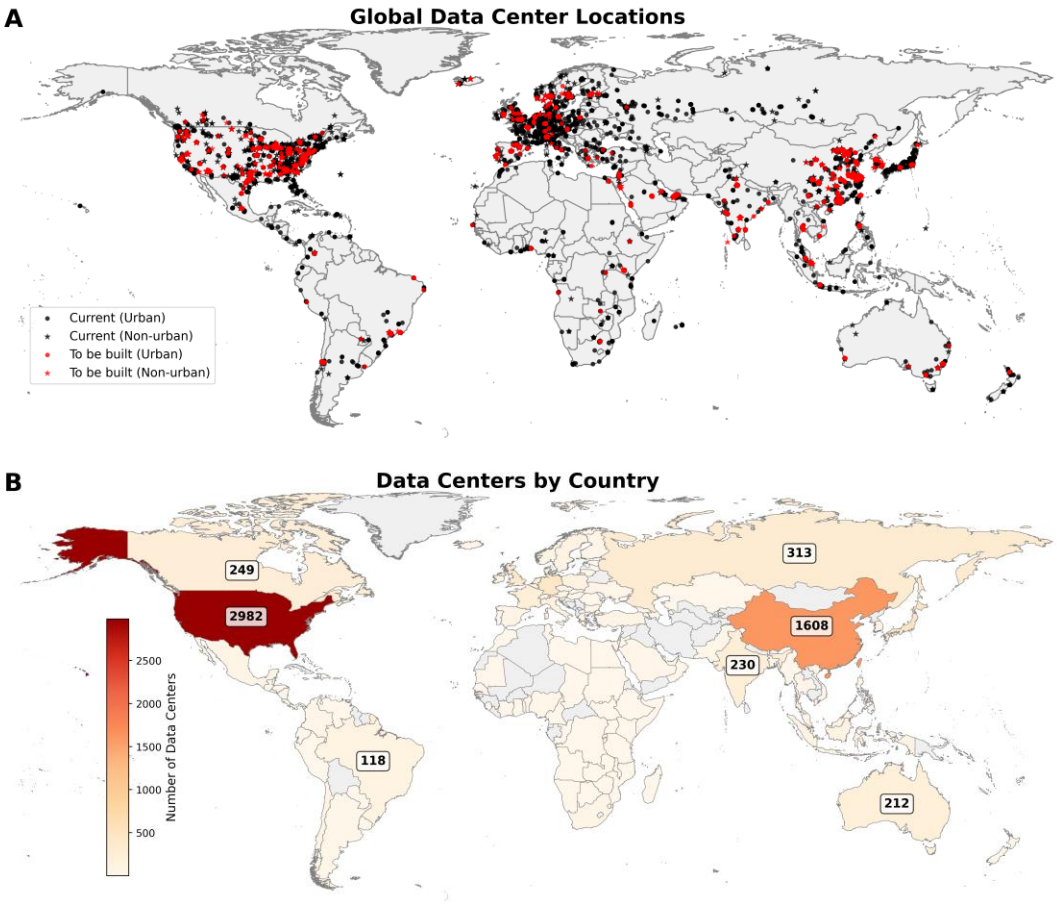

Fig. 1. Global spatial distribution of data centers. (A) Locations of 12,639 data centers analyzed in this study, highlighting clear spatial clustering across North America, Western Europe, and East Asia. Already existing facilities and those to be built are separately shown, while their overlap with global urban clusters is also characterized. Note that the exact locations are randomly shifted to protect proprietary data. (B) Total number of current data centers by country. Values are annotated for a few select cases. Dataset is current as of September 2025.

Because these facilities are increasingly sited in urban and transitioning peri-urban landscapes to secure affordable land, power, and water, they introduce heavy industrial footprints into expanding human settlements. We developed a global urban cluster database for the present (n=30,066; circa 2020 based on (*16*)) to check how these data centers are distributed across urban and rural landscapes. 81% (8,344) of the 10,296 data centers built before 2025 are within urban clusters. This percentage drops substantially (to ~52%) for clusters planned for 2025 onwards, which is intuitive given the additional space availability in peri-urban and rural areas and expected expansion of water and energy distribution systems in preparation for these planned developments.

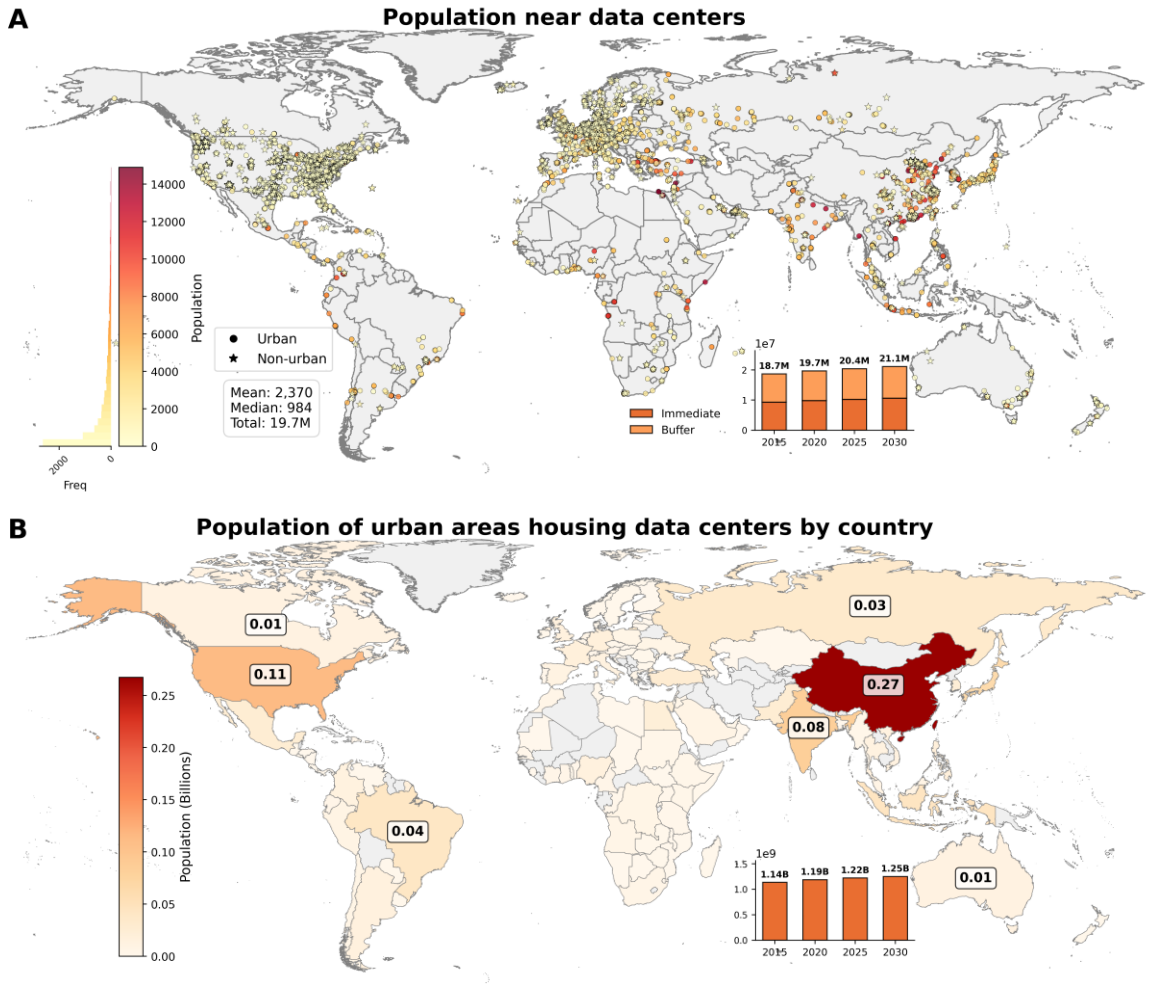

Fig. 2. Demographic proximity and population densification surrounding data centers. (A) Global distribution of human population within the microclimatic impact zones (within 300 m of unique data center location for immediate; within a further 125 m for the buffer) of data centers for 2020. Facilities are categorized by their presence or absence within present-day urban clusters. Note that the exact locations are randomly shifted to protect proprietary data. (B) Total population residing in urban clusters housing data centers by country for 2020. Values are annotated for a few select cases. Temporal trends between 2015 and 2030 are also shown as subset bar plots for both subfigures.

We also examine the potential for direct human exposure to the microclimatic shifts induced by these facilities by integrating WorldPop population grids (*17*) with localized buffers of 300 m and 425 m radius around each unique data center location, which drops the number of samples to under 8,300. These buffers are used in the subsequent section to quantify the data center heat island (DCHI) effect. In 2020, almost 20 million people lived in close proximity to data centers globally (Fig. 2A). Historical estimates and near-term population projections (*17*) suggest a persistent densification of communities near data centers, increasing from 18.7 million in 2015 to 21.1 million in 2030.

Since data centers have regional impacts through modification of water and energy demand (*4*, *6*), frequently driving up costs across larger utility grids, we also examine populations within the urban clusters that also contain one or more data centers. Over 1.14 billion people globally lived in these urban clusters in 2020, and this population is expected to increase to 1.25 billion in 2030. Roughly 110, 80, and 270 million people in the United States, India, and China, respectively, live in urban areas that also house data centers as of 2020 (Fig. 2B). Using a more physical definition of urban land (*18*) reduces these numbers slightly (Fig. S1). Overall, a substantial and growing number of us reside in direct and indirect proximity to these facilities.

The data center heat island effect

We quantify the localized thermal footprint of these facilities by analyzing 100 m resolution Landsat 8 LST observations (*19*) from 2020 to 2024. To isolate the specific impact of the data centers from broader regional UHIs or topographical variations, we calculate the DCHI intensity as the LST difference between the facility core (0–300 m radius) and a dynamically masked rural reference ring (300–425 m radius). This rural reference was strictly adjusted to exclude built environments, water bodies, and pixels with an elevation greater than ±50 m from the facility's median elevation following the standard UHI literature (*20*). We refer to this as the "baseline" algorithm (Fig. S2A).

Our findings reveal a distinct, pervasive DCHI effect. Annually, data centers show a mean localized surface warming of 0.95 °C (median of 0.81 °C) relative to their immediate natural surroundings (Fig. 3A). Notably, this localized heating is consistently seen across the globe, with 81.7% of all analyzed facilities exhibiting a positive DCHI intensity. We also compare other algorithms to isolate the DCHI effect (Fig. S2), all of which show consistently positive values (see Methods for more details; Figs S3, S4, S5). Of note, the "rural unadjusted" algorithm, which uses no land cover or topographical mask for the background reference, represents the lowest bound of the DCHI effect (Fig. S2B). Interestingly, the DCHI intensity using this algorithm is higher for the data centers outside urban clusters (mean of 0.46 °C) than for those inside (mean of 0.21 °C). On the other hand, for the "baseline" algorithm, the DCHI intensity is higher for data centers within urban clusters (mean of ~1 °C) than those outside (0.74 °C). This is intuitive because the unadjusted backgrounds already contain warmer built surfaces that artificially shrink the relative surface temperature gap, whereas the baseline algorithm filters out those pixels to reveal the data center's true thermal impact compared to natural land cover.

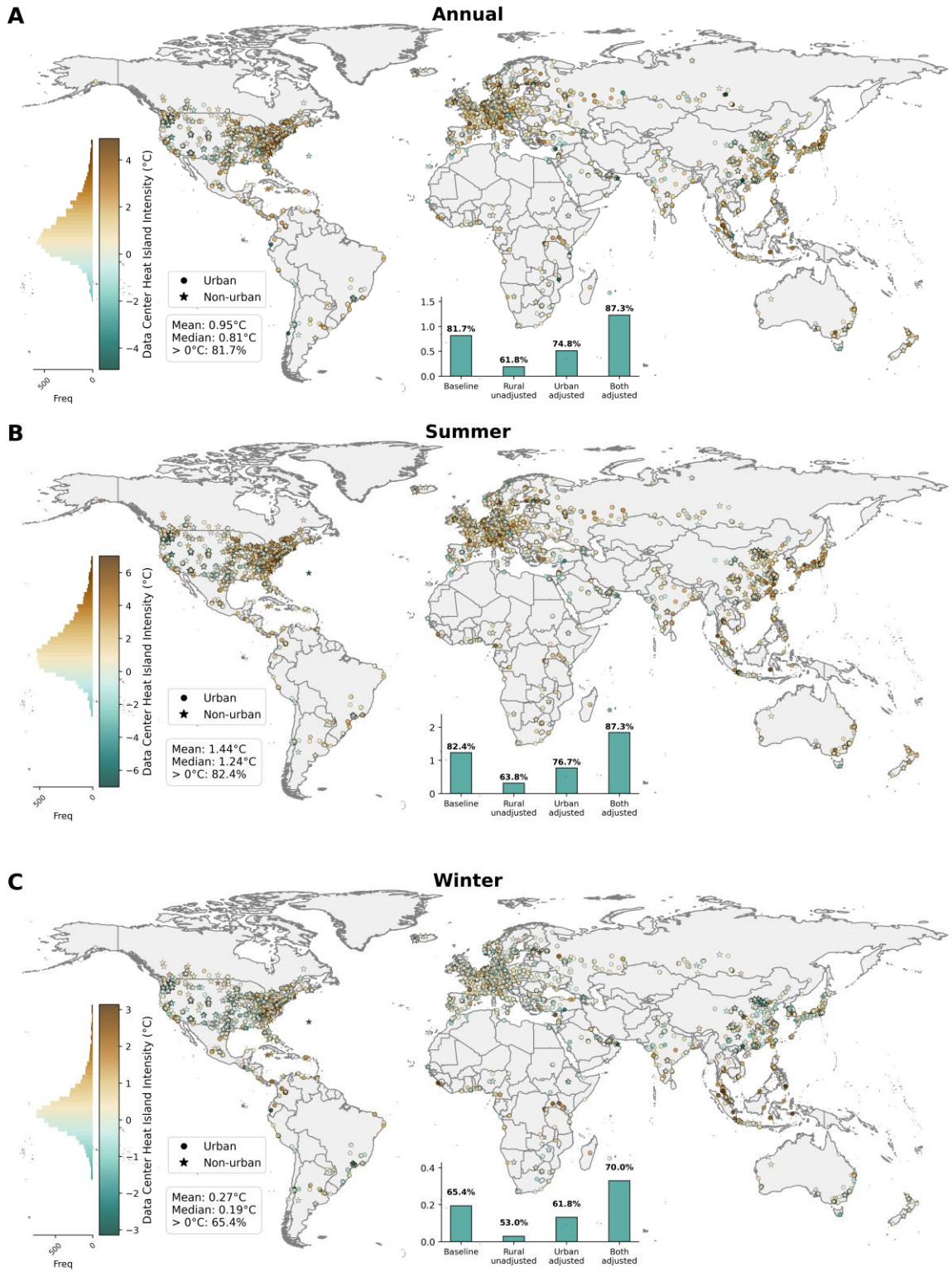

Fig. 3. The Data Center Heat Island effect. Distributions of the localized land surface temperature (LST) difference between the data center facility core (0–300 m radius) and the dynamically masked, topography-controlled rural reference ring (300–425 m radius), representing

the Data Center Heat Island (DCHI) effect for (A) annual, (B) summer, and (C) winter for 2020 to 2024. Positive values signify a facility that is warmer than its immediate surroundings. Facilities are categorized by their presence or absence within present-day urban clusters. Note that the exact locations are randomly shifted to protect proprietary data. The median DCHI and percentage of positive DCHI values for various algorithms are shown in the subset bar plots.

The intensity of this local thermal anomaly is season dependent, consistent with patterns found for the regular surface UHI effect (*21*). During the summer months (June–August for northern hemisphere and December–February for southern hemisphere), background temperatures and solar insolation peak, maximizing surface temperature differences between built and natural surfaces (Fig. 3B). Consequently, the summer DCHI intensity is higher during this season, reaching a global mean of 1.44 °C and a median of 1.24 °C (mean of 0.44 °C for the "rural unadjusted" algorithm). During this period, 82.4% of data center locations experienced local surface warming. In contrast, during winter (June–August for southern hemisphere and December–February for northern hemisphere), the DCHI intensity reduces to 0.27 °C (Fig. 3C). However, across seasons, even for our lower bound estimate, most data centers show this DCHI effect, demonstrating that they generally alter the local surface energy balance resulting in higher temperatures.

Beyond the different algorithms used, we confirm the presence of the DCHI through multiple sensitivity tests. This includes using various buffer sizes that cover the range of expected spatial extent of typical data centers (Figs S6, S7), using different averaging windows to minimize signals for years before data center construction completion (Fig. S8), and using a different open source data center location database (*22*) (albeit only for the United States; Fig. S9).

Data center-induced localized vegetation reductions

Data center construction, especially for hyperscale and enterprise facilities, necessitates converting vast tracts of land into contiguous impervious surfaces, replacing natural landscapes with server halls, substations, and logistical infrastructure. We examine this ecological degradation using the Normalized Difference Vegetation Index (NDVI), a satellite-derived proxy for live green vegetation on the surface (*23*). The extent of the ecological degradation is quantified as the NDVI gap between the facility core and the surrounding adjusted rural reference (Fig. 4). Our analysis indicates a consistent suppression of local photosynthetically active vegetation in and around data centers. Globally, data centers exhibit a mean annual NDVI gap of −0.145 (median of −0.140). 94.6% of all facilities demonstrate this negative NDVI anomaly, underscoring that local vegetation removal is often a necessity for data center development.

During the summer season (Fig. 4B), this vegetation gap is starker, with a mean summer NDVI gap of −0.163 (median: −0.154) and 94.5% of facilities displaying this gap. The magnitude of the NDVI gap is smaller in winter (mean of −0.109; median of −0.092), but still pervasive (Fig. 4C). Most data centers (between 65.7% and 69.5% depending on season) show this local negative greenness anomaly for the "rural unadjusted" algorithm, and this NDVI gap persists across all tested algorithms (Figs S10, S11, S12).

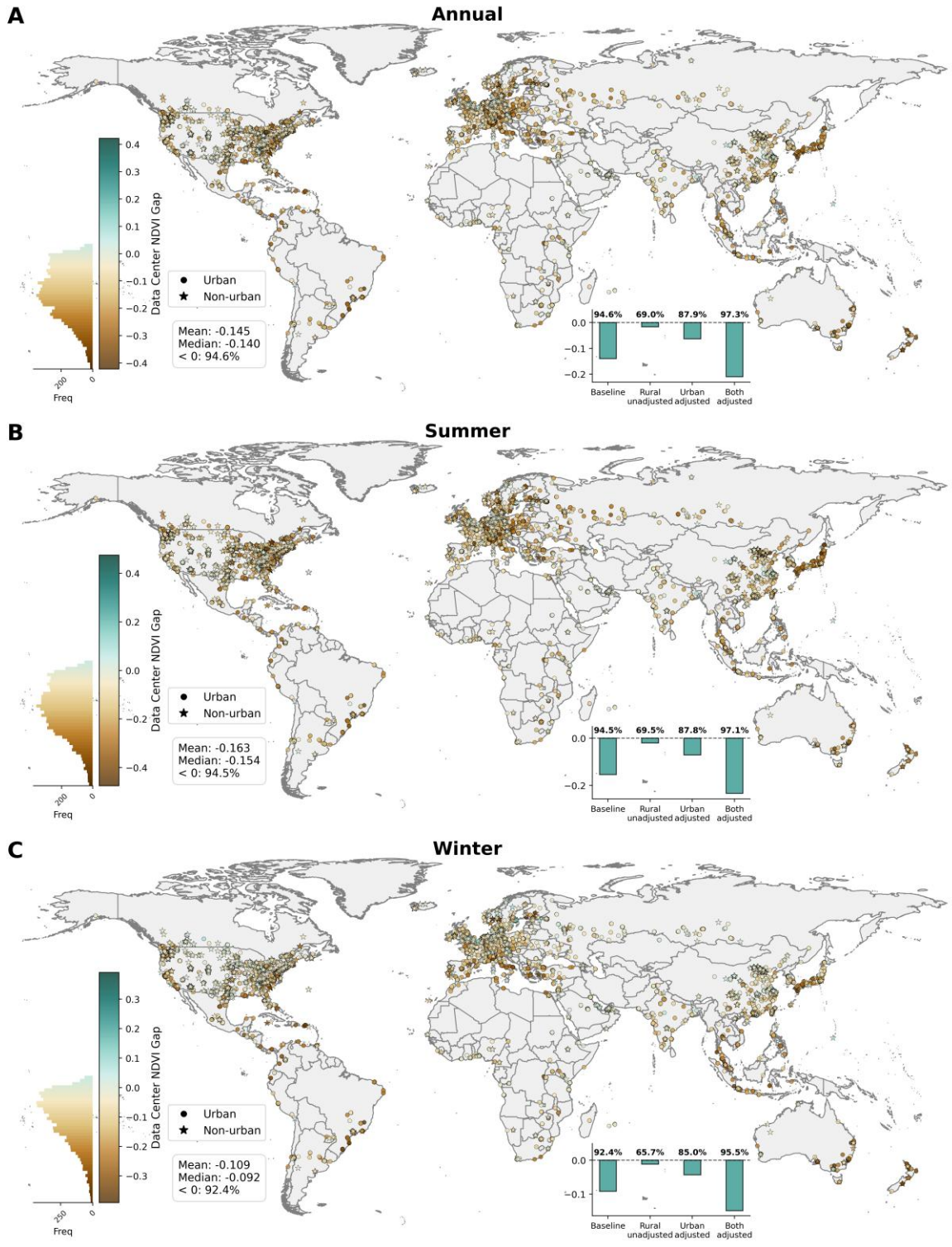

Fig. 4. Data center-induced localized vegetation reduction. Distributions of the localized Normalized Difference Vegetation Index (NDVI) gap between the data center facility core (0–300 m radius) and the dynamically masked, topography-controlled rural reference ring (300–425 m radius) for (A) annual, (B) summer, and (C) winter for 2020 to 2024. Positive values signify a

facility that is greener than its immediate surroundings. Facilities are categorized by their presence or absence within present-day urban clusters. Note that the exact locations are randomly shifted to protect proprietary data. The median NDVI gap and percentage of negative NDVI gaps for various algorithms are shown in the subset bar plots.

The DCHI effect is strongly modulated by this local vegetation reduction, with the variability of DCHI across data center locations significantly associated ($p<0.005$) with the corresponding NDVI gap for almost all cases (Fig. S13). The correlations are generally strongest during summer, with the coefficient of determination (R^2) varying between 0.267 and 0.452 (Fig. S13B), and weakest during winter (Figs S13C, S13F). Additionally, the correlations between the two anomalies are stronger for data centers in non-urban locations compared to the urban ones. These associations are conceptually grounded since the lower evaporative cooling due to vegetation reduction would mechanistically lead to the observed thermal anomalies (*24*).

Discussion

The rapid proliferation of global data centers necessitates a fundamental reevaluation of their environmental footprint. While the energy, water, and carbon demands of hyperscale computing are widely recognized (*3, 6, 25*), our findings demonstrate that data centers also act as potent, localized drivers of land cover conversion and microclimatic warming. Crucially, our spatial demographic analysis reveals that these physical impacts are not isolated to unpopulated hinterlands. Rather, they are increasingly happening in growing human settlements (*11, 26*), directly amplifying the potential for human exposure to localized environmental stressors while reducing access to ecosystem services (*8*).

The observed thermal anomalies mainly stem from the replacement of natural, vegetated landscapes with highly impervious surfaces (Fig. S13). In a natural vegetated landscape, absorbed solar radiation is largely dissipated as latent heat through evapotranspiration. By reducing local vegetation, data center construction suppresses this evaporative cooling mechanism, forcing the environment to dissipate energy primarily as sensible heat (*10*). In theory, the local thermal anomaly may be further exacerbated by the continuous, high-intensity emission of anthropogenic waste heat from server cooling systems (*12, 27*). However, our analysis did not find any substantial association between the DCHI intensity and the utilized uninterruptible power supply of the data center (Fig. S14), which the anthropogenic waste heat should scale with. This may be because the anthropogenic heat flux, although large, is still localized compared to the impact of the large-scale surface conversion due to data center construction. This is also confirmed when only looking at LST differences between built pixels within the facility core and those in their immediate surroundings (Table S1). However, since these are purely observational estimates at large scales influenced by many confounders, we encourage the use of finer-scale modeling tools to isolate the impacts of these two mechanisms in future studies. Importantly, our estimates are constrained to daytime, and the effect of the anthropogenic emissions on the microclimate may be more

noticeable during stable nights (*12*, *28*), when these data centers are still continuously running and ejecting heat.

Developers frequently prefer to site data centers in locations with easy access to water for cooling and energy distribution systems (*26*). As such, the majority (81%) of these data centers are located within urban environments, where they cause land use changes that directly intersect with expanding population centers. Consequently, communities densely populated within the microclimate of these facilities (Fig. 2) could face direct impacts (*29*), paralleling the impacts of standard urban heat islands (*30*). Globally, around 1.14 billion residents live in urban environments hosting data centers as of 2020. Thus, beyond the potential localized thermal impacts on adjacent populations, which are particularly amplified during hot summers (Fig. 3B), these facilities can trigger indirect urban-scale impacts by driving up costs for land, energy, and water; an aspect that has been widely reported on *(3, 6, 9, 17*).

Overall, these localized microclimatic shifts due to data centers may cascade into broader hydrological and ecological systems. Since data centers sometimes rely on water-intensive evaporative cooling to manage thermal loads, the extreme localized summer warming we observe may diminish the efficiency of ambient air-side cooling. This may create a positive feedback loop that forces a higher reliance on local water resources precisely when seasonal scarcity peaks. Concurrently, the extensive sealing of soils may alter watershed dynamics by accelerating surface runoff and preventing the aquifer recharge that these facilities often depend upon (*31*). Ecologically, the physical footprint of these facilities can drive habitat fragmentation (Fig. 4). Unlike mixed-use urban development that may retain fragmented green spaces, especially with increasing focus on urban greening (*32*), the highly secured, purely functional perimeters of data center facilities often offer little ecological refuge.

The computationally intensive demands of artificial intelligence and cloud computing almost guarantee that the physical footprint of data centers will continue to expand at an unprecedented rate (*4, 33*). Mitigating these impacts requires expanding environmental assessments beyond macro-level carbon and energy accounting to include strict mandates for local microclimatic, ecological, and human exposure preservation. Mandating local green infrastructure, transitioning to closed-loop liquid cooling to preserve watersheds, and implementing waste-heat recovery systems to benefit surrounding settlements are essential steps. Recognizing and addressing the localized environmental and demographic consequences of this digital age is critical to ensuring sustainable development for future computing infrastructure as it competes for land and resources traditionally allocated for human settlements.

While the global analysis presented here illustrates the currently understudied localized microclimate and ecological impacts of data centers, it is important to note key limitations. First, the space-for-time algorithm developed to estimate the DCHI makes uniform assumptions about the data center footprint due to a lack of information regarding exact facility boundaries. So, if, for instance, the data center was built on a pre-existing barren lot, the NDVI and LST gaps seen

here may not be a unique consequence of data center construction. Although using different buffer sizes confirms the persistence of the DCHI effect (Figs S6, S7), the measurable magnitude of this effect ultimately depends on our ability to resolve the spatial extent of these facilities. Second, the DCHI effect is estimated using satellite-derived LST, which is not as direct a proxy for human-scale heat hazard as ambient air temperature (*34*). Based on the thermodynamic coupling between air temperature and LST, DCHI for air temperature should theoretically exist, but would be much smaller in magnitude than those estimated from LST (*34*). Given the lack of global fine-grain air temperature datasets that can resolve data center impacts on microclimate, localized field assessments remain essential (*12*). Specifically, future work must quantify the impact of data centers on ambient air temperature and other factors modulating heat stress, most notably humidity (*35*), which may be significantly altered by the use of large-scale evaporative cooling systems. Finally, while population estimates are more reliable at the bulk urban scale, the global datasets used here do not adequately capture intra-urban variability, nor were they developed to account for the relocation of existing populations due to data center build-up. Of note, hyperscale data centers are highly secured, fenced-off industrial zones with virtually zero residential density inside the perimeter. As such, we expect the immediate population estimates in this study to overstate the populations actively at risk. Even with these uncertainties in mind, our empirical estimates strongly support our conceptual expectations of local thermal anomalies driven by the physical presence of data centers, serving as a vital starting point for informing the sustainable future growth of digital infrastructure in our physical spaces.

Materials & Methods

Data center locations

The precise geographical coordinates and metadata for 13,587 global data centers were sourced from a newly compiled proprietary geospatial database by S&P Global (*15*), which aggregates industry registries and cloud-provider infrastructure footprints. The dataset includes not just the location of data centers, but also the year the facility was built and the uninterruptible power supply, among other metadata. Of these, some facilities are sub-facilities that fall under parent facilities, which reduces the sample size to 12,639. All geoprocessing and large-scale raster computations were conducted utilizing the Google Earth Engine cloud computing platform (*36*). Since some of these data centers operate out of the same facility, or their locations may have been miscoded in the property dataset, we only use unique latitude longitude pairs when examining the thermal and ecological effects, which drops our sample size to around 8,300. Note that the exact sample size is around 8,000 for all the analysis but varies due to missing data for satellites (for instance, due to cloud contamination over some data center locations), which varies by variable and season. Although all of the geospatial analysis (see subsection below) used the actual location of the data centers, the maps shown here (Figs 1, 2, 3, 4, S1, S3, S4, S5, S10, S11, S12) randomly shift these locations during visualization to protect the integrity of the proprietary information.

Processing global satellite data

To quantify the localized microclimatic and ecological signals, we utilized medium-resolution (30 to 100 m) Landsat 8 imagery (*19*). From these, Land Surface Temperature (LST) (*37*) was derived from the thermal infrared sensor, which provides atmospherically corrected LST at 100 m resolution corresponding to roughly 10:30 am local time. The Normalized Difference Vegetation Index (NDVI) (*23*), a proxy for live green vegetation on the surface, was calculated using the surface reflectance values of the near-infrared and red optical bands at 30 m resolution. To ensure data fidelity, we applied rigorous cloud and cloud-shadow masking using the pixel-level quality control flags, retaining only clear-sky observations. Three primary climatological baselines were established by averaging all available clear-sky Landsat 8 images between January 1, 2020, and December 31, 2024. They were: 1) an annual composite encompassing all months, 2) a summer-season composite filtered by calendar month (June through August for the Northern Hemisphere and December through February for Southern Hemisphere), and 3) a winter-season composite (December through February for Northern Hemisphere and June through August for Southern Hemisphere).

Space-for-time isolation localized environmental impacts of data centers

A fundamental challenge in quantifying isolated microclimatic anomalies is distinguishing the target facility's signal from background geographical and urban variations. We implemented a spatial buffer methodology to isolate the exact thermal and vegetative footprint of the data centers. For each facility coordinate, we defined a “facility core” using a circular buffer area with a 300 m radius, representing the immediate physical footprint and highly disturbed localized environment

of the data center. The radius of this circular buffer was decided to both account for the upper bound of the operational area of hyperscale data centers in the S&P Global database, which is 0.172 million m^2, and to allow enough pixels to have a sufficient sample size for each estimate. A surrounding "rural" reference buffer was established as an outer ring stretching from 300 m to 425 m. This rural reference ring would have roughly the same area as the 300 m circular buffer. To prevent confounding signals from neighboring human settlements or extreme topography, the rural reference ring was dynamically adjusted and masked for each individual facility. First, we utilized the European Space Agency (ESA) WorldCover (10 m resolution) (*38*) dataset to mask out all existing built environments, water bodies, and snow/ice from the rural ring, ensuring the reference represented a typical natural or agricultural baseline. Second, we applied a strict topographic control using the United States Geological Survey's Global Multi-resolution Terrain Elevation Data (*39*). The median elevation of the 300 m facility core was calculated; any pixel in the surrounding rural buffer with an elevation difference exceeding ±50 m from this center median was masked out, following similar approaches used in the urban heat island literature (*40*). This eliminated temperature discrepancies driven purely by elevation differences and sloped terrain.

The Data Center Heat Island (DCHI) intensity and the localized NDVI gap were calculated using a space-for-time approach (*41*), as the difference in median values between the facility core and its surrounding topography-controlled rural buffer. A positive DCHI indicates a facility is warmer than its natural surroundings, while a negative NDVI gap indicates a reduction in local vegetation relative to the immediate reference area.

Different algorithms, statistical analyses, and sensitivity tests

In addition to our baseline algorithm, we developed three additional algorithms to estimate the DCHI intensity and NDVI gap (Fig. S2). First, the "rural unadjusted" approach calculates the LST and NDVI of the outer rural buffer without applying any standard elevation constraints or natural land cover masks. Second, the "urban adjusted" approach calculates the LST and NDVI for only the built-up pixels based on the ESA WorldCover (*38*) within the facility core, thereby minimizing the cooling influence of any on-site landscaping or vegetation. Third, the "both adjusted" approach utilizes both the masked rural reference and the built pixels within the facility core to get the upper bound Δ between the data center location and its natural surroundings.

We examine associations between the DCHI intensity and the NDVI gap for all cases, finding moderately strong negative relationships between them, with the strongest associations in summer (Fig. S13). We also examine whether the DCHI intensity across facilities is associated with their corresponding average utilized uninterruptible power supply (UPS), which should broadly scale with its energy dissipation due to cooling requirements. The associations seen are incredibly weak (Fig. S14). This suggests that the DCHI is primarily due to the land cover conversion, not the heat exhaust from data centers, at least at the scales examined here. Note that the associations here are

probably further weakened due to the uncertainties in the UPS data, which is only reported in large step sizes and not on a continuous scale, and also does not represent actual energy utilization.

Beyond the different algorithms used, we confirm the existence of the DCHI through multiple sensitivity tests.

Our baseline extraction utilizes a 300 m circular buffer and a 300–425 m rural reference ring, which provides sufficient Landsat pixels (~28) to get robust estimates of the LST signals. Because data center footprints vary widely, with our facility core, covering around 0.283 million m^2, generally expected to be bigger than most operational data centers, we tested two reduced spatial configurations to better align with the expected spatial extent of typical facilities. One used a 100 m center with a 100–150 m rural reference ring, while the other used a 200 m center with a 200–300 m rural reference ring. Similarly to account for potentially larger facilities or a footprint effect from these land cover conversions, we also consider two sets of larger spatial configurations. The first one used a 400 m center with a 400–575 m rural reference ring, while the second used a 500 m center with a 500–725 m rural reference ring. While the magnitude of the DCHI and NDVI gap are, expectedly, different, for all of these different area assumptions (shown for summer and winter in Figs S6, S7), and across all algorithms tested, the signals clearly persist.

Our baseline analysis utilizes a five-year mean (2020–2024) of Landsat 8 observations to ensure high-quality, cloud-free composites. To ensure our thermal signal was not diluted by imagery captured prior to the completion of newer data centers, we reran the analysis using several other averaging windows, namely 2021–2024, 2022–2024, 2023–2024, and only for 2024 (Fig. S8). The DCHI signals are seen in all cases. The monotonic decrease in the DCHI intensity in almost all cases with shorter (and more recent) averaging windows is probably due to a combination of two reasons. First, the presence of data centers (or the anticipation of future data center operation during its construction) is leading to urban development in its surroundings, meaning the rural reference is warming up faster than the already established data center. Second, since the ESA WorldCover data is for 2020, it cannot detect land cover transition from natural to built-up in the surrounding rural reference, while the Landsat is detecting the warmer built surface for the more recent years.

Finally, to ensure our results were not an artifact of the uncertainties inherent in our primary propriety dataset, we replicated the baseline analysis using an alternative, open-source data center location database (*22*), though this specific validation was limited to the United States due to data availability.

To test if data centers uniquely generate more local warming than typical impervious surfaces, we recalculated DCHI using only the built pixels in both the facility core and the rural reference ring. Doing so allows us to check whether the built pixels associated with data centers are warmer than

those in the surrounding region. Our analysis shows that the data center built pixels are barely, if at all, warmer than the surrounding built pixels, with only around half of the facilities showing any additional warming, which can be attributed to chance (Table S1). We should note that while this is indicative that data centers are not causing any additional warming compared to regular built infrastructure at global scales, it is not definitive since the ESA WorldCover data does not account for faster build up, and thus warming, of the surroundings after data center construction. However, the results do not change substantially when only considering data centers built before 2020. Intuitively, one might expect stronger impacts of data center on local temperatures due to the dissipation of anthropogenic heat, which has been seen for some urban areas (*28, 42*), and suggested for regions with high data center density (*12*). However, separating out the land cover effect of data centers from their anthropogenic heat emissions on local microclimate requires more advanced modeling tools. Furthermore, while the results in Table S1 are consistent with the weak associations seen between DCHI and UPS in Fig. S14, UPS remains an imperfect proxy for actual thermal exhaust. Different cooling technologies (evaporative versus air-side versus mechanical) would interact with the local microclimate in fundamentally different ways (increasing humidity versus air temperature), further supporting the importance of process-based modeling to isolate the impacts of data centers.

Demographic and urban characterization

To quantify the human population exposed to data center microclimates, we integrated the WorldPop global high-resolution population dataset (*17*). Population sums were extracted for five-year intervals (2015, 2020, 2025, and 2030) across both the 300 m facility core and the 300–425 m rural reference ring. To account for highly concentrated data center hubs and prevent the double-counting of exposed populations, we utilized the Global Human Settlement Layer (GHSL) dataset (*16*). First, the contiguous groups of medium density class pixels were vectorized to create a global dataset of over 30,000 urban clusters (*20*). A spatial join was then applied to intersect data center locations with these clusters to estimate which of the data centers were housed within urban environments. For any given GHSL cluster containing multiple data centers, the total population of that urban boundary was extracted and assigned exclusively to the primary facility index, with duplicate counts within the same cluster zeroed out. Since there are various ways to define urban areas, with GHSL considering a combination of demographic and physical urbanization, we also developed another urban cluster dataset by vectorizing contiguous built-up pixels from the European Space Agency Climate Change Initiative land cover data (*18*) for 2020 and reran the analysis. These clusters represent purely physical urbanization and show somewhat smaller, but still in the billions, count of people with data centers housed in their urban environments. Finally, a spatial intersection with World Bank administrative boundaries (*43*) was applied to append country-level identifiers, enabling national-scale aggregations of both demographic and microclimatic data.

References

1. K. Kant, Data center evolution: A tutorial on state of the art, issues, and challenges. *Comput. Netw.* **53**, 2939–2965 (2009).

2. S. Sarkar, A. Naug, R. Luna, A. Guillen, V. Gundecha, S. Ghorbanpour, S. Mousavi, D. Markovikj, A. R. Babu, "Carbon footprint reduction for sustainable data centers in real-time" in *Proceedings of the AAAI Conference on Artificial Intelligence* (2024)vol. 38, pp. 22322–22330.

3. A. Shehabi, E. Masanet, H. Price, A. Horvath, W. W. Nazaroff, Data center design and location: Consequences for electricity use and greenhouse-gas emissions. *Build. Environ.* **46**, 990–998 (2011).

4. M. Koot, F. Wijnhoven, Usage impact on data center electricity needs: A system dynamic forecasting model. *Appl. Energy* **291**, 116798 (2021).

5. P. Wang, L. Rao, X. Liu, Y. Qi, D-Pro: Dynamic data center operations with demand-responsive electricity prices in smart grid. *IEEE Trans. Smart Grid* **3**, 1743–1754 (2012).

6. D. Mytton, Data centre water consumption. *Npj Clean Water* **4**, 11 (2021).

7. D. Al Kez, A. M. Foley, D. Laverty, D. F. Del Rio, B. Sovacool, Exploring the sustainability challenges facing digitalization and internet data centers. *J. Clean. Prod.* **371**, 133633 (2022).

8. W. M. Ngata, N. Bashir, M. Westerlaken, L. Liote, Y. Chandio, E. Olivetti, "The Cloud next door: investigating the environmental and socioeconomic strain of datacenters on local communities" in *Proceedings of the ACM SIGCAS/SIGCHI Conference on Computing and Sustainable Societies* (2025), pp. 769–774.

9. J. Monstadt, K. Saltzman, How data centers have come to matter: Governing the spatial and environmental footprint of the 'digital gateway to Europe.' *Int. J. Urban Reg. Res.* **49**, 757–778 (2025).

10. T. R. Oke, The energetic basis of the urban heat island. *Q. J. R. Meteorol. Soc.* **108**, 1–24 (1982).

11. C. Carr, D. Bast, K. Madron, A. M. Syrus, Mapping the clouds: the matter of data centers. *J. Maps* **18**, 106–113 (2022).

12. D. J. Sailor, S. S. Abolhassani, E. P. Martin, Data center waste heat as an emerging urban thermal hazard: First field measurements of neighborhood-scale air temperature impacts. *ASME J. Eng. Sustain. Build. Cities*, 1–12 (2026).

13. H. Rong, H. Zhang, S. Xiao, C. Li, C. Hu, Optimizing energy consumption for data centers. *Renew. Sustain. Energy Rev.* **58**, 674–691 (2016).

14. D. M. Lawrence, G. C. Hurtt, A. Arneth, V. Brovkin, K. V. Calvin, A. D. Jones, C. D. Jones, P. J. Lawrence, N. de Noblet-Ducoudré, J. Pongratz, S. I. Seneviratne, E. Shevliakova, The Land Use Model Intercomparison Project (LUMIP) contribution to CMIP6:rationale and experimental design. *Geosci. Model Dev.* **9**, 2973–2998 (2016).

15. S&P Global Market Intelligence, "451 Research Data Center KnowledgeBase" (S&P Global, 2025).

16. European Commission. Joint Research Centre., *GHSL Data Package 2023.* (Publications Office, LU, 2023; https://data.europa.eu/doi/10.2760/098587).

17. M. Bondarenko, R. Priyatikanto, N. Tejedor Garavito, W. Zhang, T. McKeen, A. Cunningham, T. Woods, J. Hilton, D. Cihan, B. Nosatiuk, Constrained estimates of 2015-2030 total number of people per grid square at a resolution of 3 arc (approximately 100m at the equator) R2025A version v1. (2025).

18. R. Hollmann, C. J. Merchant, R. Saunders, C. Downy, M. Buchwitz, A. Cazenave, E. Chuvieco, P. Defourny, G. de Leeuw, R. Forsberg, The ESA climate change initiative: Satellite data records for essential climate variables. *Bull. Am. Meteorol. Soc.* **94**, 1541–1552 (2013).

19. C. J. Crawford, D. P. Roy, S. Arab, C. Barnes, E. Vermote, G. Hulley, A. Gerace, M. Choate, C. Engebretson, E. Micijevic, The 50-year Landsat collection 2 archive. *Sci. Remote Sens.* **8**, 100103 (2023).

20. T. C. Chakraborty, C. Sarangi, X. Lee, Reduction in human activity can enhance the urban heat island: insights from the COVID-19 lockdown. *Environ. Res. Lett.* **16**, 054060 (2021).

21. N. Clinton, P. Gong, MODIS detected surface urban heat islands and sinks: Global locations and controls. *Remote Sens. Environ.* **134**, 294–304 (2013).

22. K. Mongird, T. Thurber, C. Vernon, C. Burleyson, K. Z. Akdemir, J. Rice, IM3 Open Source Data Center Atlas, Pacific Northwest National Lab (United States); https://doi.org/10.57931/2550666.

23. N. Pettorelli, *The Normalized Difference Vegetation Index* (Oxford University Press, 2013).

24. A. Paschalis, T. C. Chakraborty, S. Fatichi, N. Meili, G. Manoli, Urban Forests as Main Regulator of the Evaporative Cooling Effect in Cities, *AGU Adv*. **2** (2021)p. e2020AV000303.

25. A. Shehabi, S. Smith, D. Sartor, R. Brown, M. Herrlin, J. Koomey, E. Masanet, N. Horner, I. Azevedo, W. Lintner, United states data center energy usage report. (2016).

26. P. T. Jaeger, J. Lin, J. M. Grimes, S. N. Simmons, Where is the cloud? Geography, economics, environment, and jurisdiction in cloud computing. *First Monday* (2009).

27. X. Li, L. Zhao, Y. Qin, K. Oleson, Y. Zhang, Elevated urban energy risks due to climate-driven biophysical feedbacks, *Nat. Clim. Change*. **14** (2024). https://doi.org/10.1038/s41558-024-02108-w.

28. F. Salamanca, M. Georgescu, A. Mahalov, M. Moustaoui, M. Wang, Anthropogenic heating of the urban environment due to air conditioning, *J. Geophys. Res. Atmos.* **119** (2014)pp. 5949–5965.

29. N. Gour, L. Ortiz, E. Maibach, Health implications of the rapid rise of data centers in Virginia: an exploratory assessment. *Front. Clim.* **8**, 1648912 (2026).

30. S. Wang, W. Zhan, B. Zhou, S. Tong, T. Chakraborty, Z. Wang, K. Huang, H. Du, A. Middel, J. Li, Z. Liu, L. Li, F. Huang, M. Li, Dual impact of global urban overheating on mortality. *Nat. Clim. Change* **15**, 497–504 (2025).

31. W. D. Shuster, J. Bonta, H. Thurston, E. Warnemuende, D. R. Smith, Impacts of impervious surface on watershed hydrology: A review. *Urban Water J.* **2**, 263–275 (2005).

32. J. Chen, B. Qiu, T. C. Chakraborty, X. Miao, Y. Cao, L. Li, S. Zhao, Y. Ni, X. Tian, Y. Qian, Contrasting effects of urbanization on vegetation between the Global South and Global North. *Nat. Sustain.*, 1–12 (2025).

33. A. Shehabi, S. J. Smith, E. Masanet, J. Koomey, Data center growth in the United States: decoupling the demand for services from electricity use. *Environ. Res. Lett.* **13**, 124030 (2018).

34. Z. S. Venter, T. Chakraborty, X. Lee, Crowdsourced air temperatures contrast satellite measures of the urban heat island and its mechanisms. *Sci. Adv.* **7**, eabb9569 (2021).

35. J. W. Baldwin, T. Benmarhnia, K. L. Ebi, O. Jay, N. J. Lutsko, J. K. Vanos, Humidity's Role in Heat-Related Health Outcomes: A Heated Debate. *Environ. Health Perspect.* **131**, 055001 (2023).

36. N. Gorelick, M. Hancher, M. Dixon, S. Ilyushchenko, D. Thau, R. Moore, Google Earth Engine: Planetary-scale geospatial analysis for everyone. *Remote Sens. Environ.* **202**, 18–27 (2017).

37. M. Jin, R. E. Dickinson, Land surface skin temperature climatology: benefitting from the strengths of satellite observations. *Env. Res Lett* **5**, 044004 (2010).

38. D. Zanaga, R. Van De Kerchove, W. De Keersmaecker, N. Souverijns, C. Brockmann, R. Quast, J. Wevers, A. Grosu, A. Paccini, S. Vergnaud, *ESA WorldCover 10 m 2020 V100, Zenodo* (2021).

39. J. J. Danielson, D. B. Gesch, *Global Multi-Resolution Terrain Elevation Data 2010 (GMTED2010)* (US Department of the Interior, US Geological Survey, 2011).

40. Q. Yang, Y. Xu, X. Tong, X. Huang, Y. Liu, T. Chakraborty, C. Xiao, T. Hu, An adaptive synchronous extraction (ASE) method for estimating intensity and footprint of surface urban heat islands: A case study of 254 North American cities. *Remote Sens. Environ.* **297**, 113777 (2023).

41. J. L. Blois, J. W. Williams, M. C. Fitzpatrick, S. T. Jackson, S. Ferrier, Space can substitute for time in predicting climate-change effects on biodiversity. *Proc. Natl. Acad. Sci.* **110**, 9374–9379 (2013).

42. T. Ichinose, K. Shimodozono, K. Hanaki, Impact of anthropogenic heat on urban climate in Tokyo. *Atmos. Environ.* **33**, 3897–3909 (1999).

43. World Bank, World Bank Country and Lending Groups (2023). https://datahelpdesk.worldbank.org/knowledgebase/articles/906519-world-bank-country-and-lending-groups.

Acknowledgments

Funding: This research has been supported by the U.S. Department of Energy Office of Science Biological and Environmental Research program area through an Early Career Research Grant and by the Integrated Multisector, Multiscale Modeling (IM3) project. PNNL is operated for the Department of Energy by Battelle Memorial Institute under contract DE-AC05-76RL01830.

Author contributions: T.C. designed the study, processed all the observations, analyzed the data, and wrote the manuscript.

Competing interests: The author has no competing interests.

Data and materials availability: While the raw S&P Global data center dataset used in this analysis is proprietary, all the estimates of data center heat islands and normalized difference vegetation index gaps using various algorithms, sans any metadata, will be publicly released on publication of this manuscript. The IM3 Open Source Data Center Atlas, which is also used to estimate the data center heat island intensity as a sensitivity test, can be assessed here: https://doi.org/10.57931/2550666

Supplementary Materials

Figs. S1 to S14

Supplementary Materials for

Local heat islands and vegetation losses are microclimatic consequences of global data centers

TC Chakraborty[1,*]

[1]Pacific Northwest National Laboratory, Richland, WA, USA

*Corresponding author: TC Chakraborty, Email: tc.chakraborty@pnnl.gov

This PDF file includes:

Figs. S1 to S14

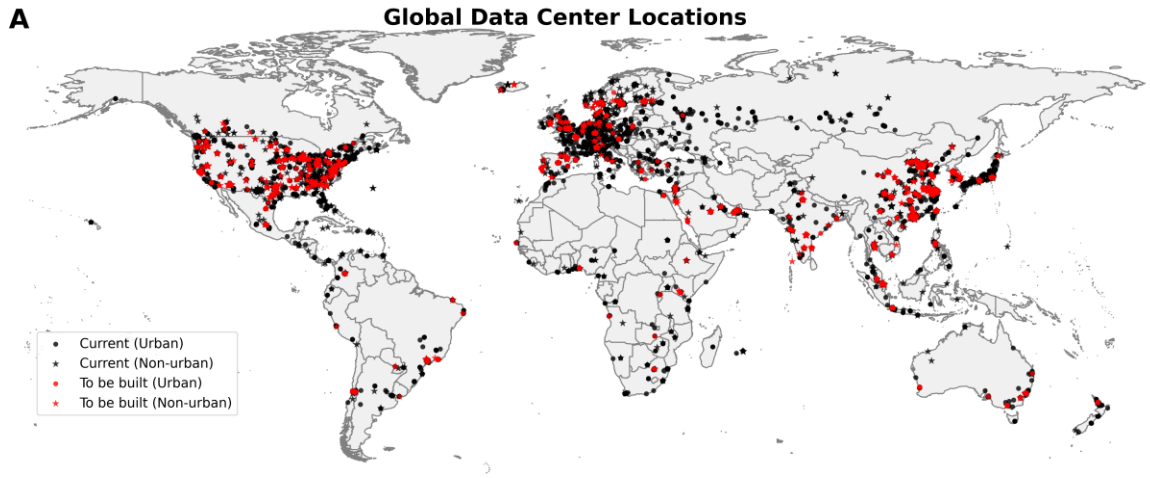

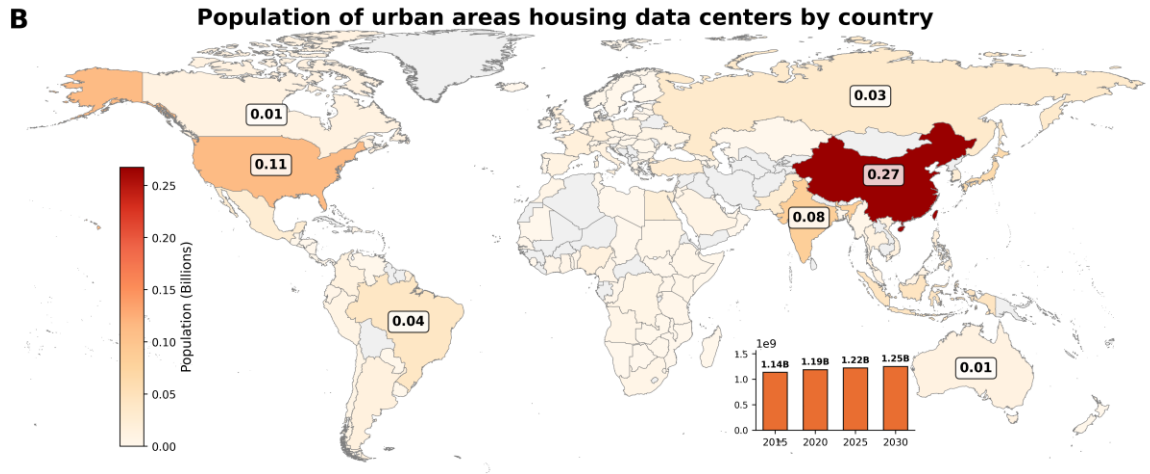

Fig. S1. Data center distribution and population densification using alternative urban definition. (A) Locations of 12,639 data centers analyzed in this study. Their overlap with global urban clusters created by vectorizing the European Space Agency Climate Change Initiative land cover data for 2020 is also characterized. Already existing facilities and those to be built are separately shown. Note that the exact locations are randomly shifted to protect proprietary data. (B) Total population residing in these urban clusters housing data centers by country for 2020. Values are annotated for a few select cases. Temporal trends between 2015 and 2030 are also shown as a subset bar plot.

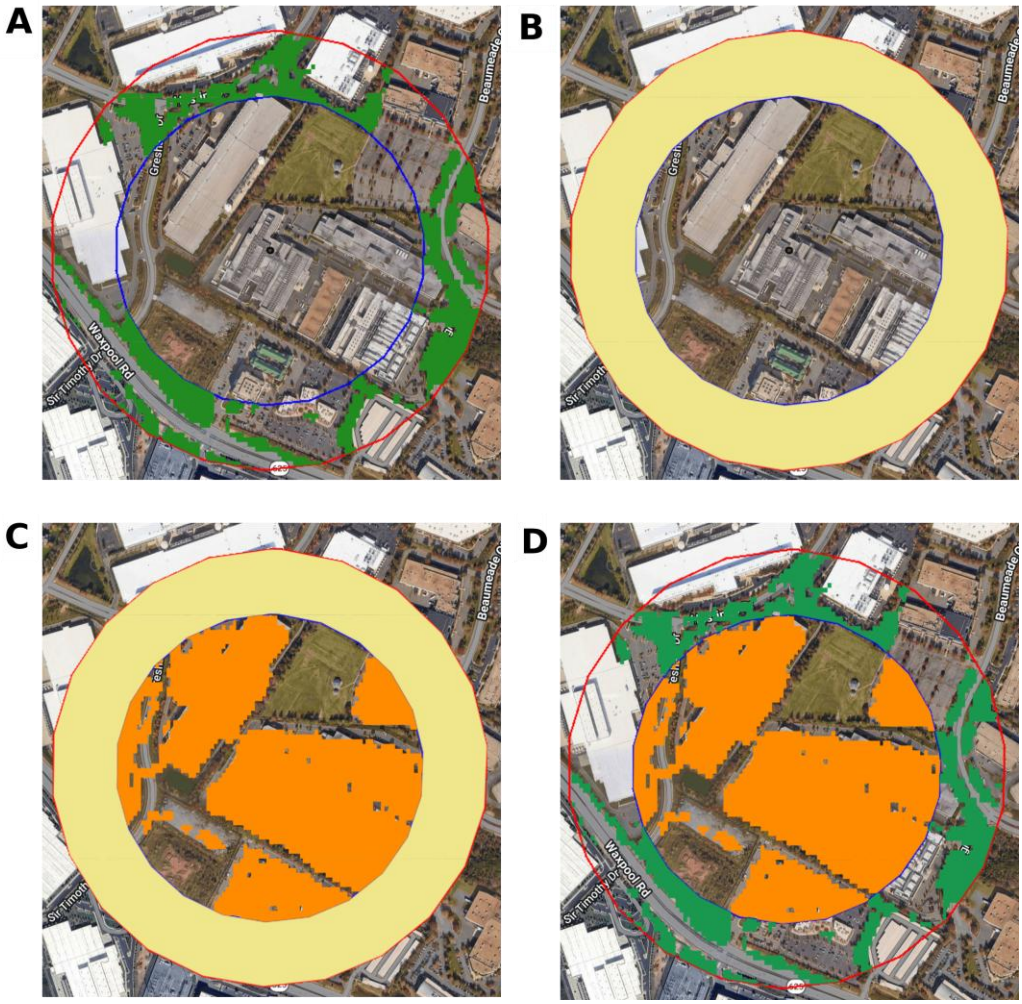

Fig. S2. Illustration of algorithms to estimate data center impacts. Aerial imagery of a representative data center in Ashburn, Virginia demonstrating the various algorithms we developed to calculate data center heat island intensity and vegetation reduction. The inner blue boundary defines the 300-m "facility core," while the outer red boundary demarcates the 300–425 m surrounding rural reference ring. (A) Derivation of the baseline topography-controlled rural reference buffer (green). To establish a natural baseline, pixels within the reference ring are filtered using ESA WorldCover to exclude existing built environments and water bodies, and constrained to eliminate topographic differences exceeding ±50 m from the median elevation of the facility core. (B) The "rural unadjusted" approach (yellow), which utilizes the entire outer reference ring without applying any land-cover masks or elevation constraints. (C) The "urban adjusted" approach, which isolates built-up pixels within the facility core (orange), compared against the unadjusted rural reference. (D) The "both adjusted" approach. This calculates the upper-bound Δ by comparing only the built-up pixels within the facility core (orange) against the strictly masked, topography-controlled rural reference (green). Map data: Google Earth.

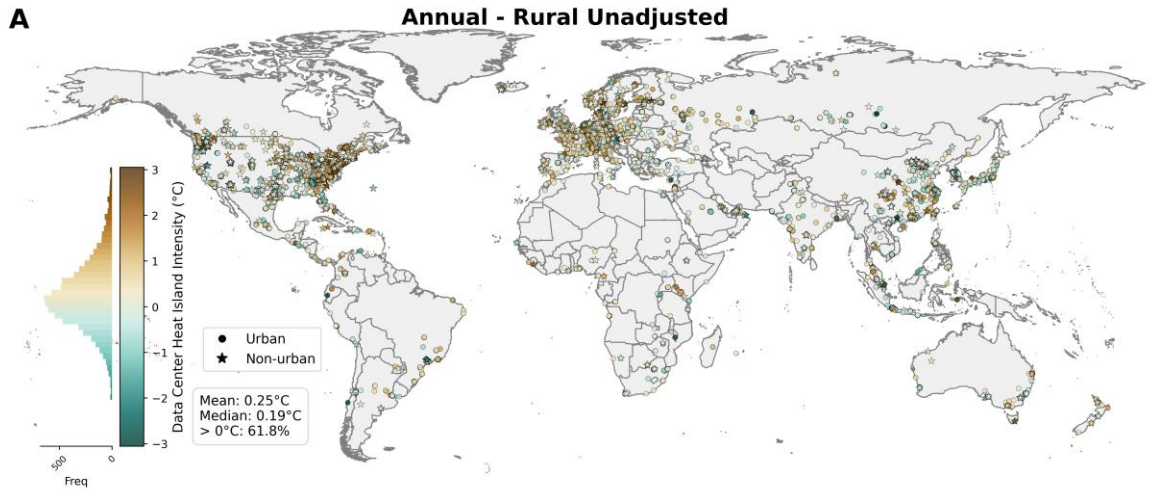

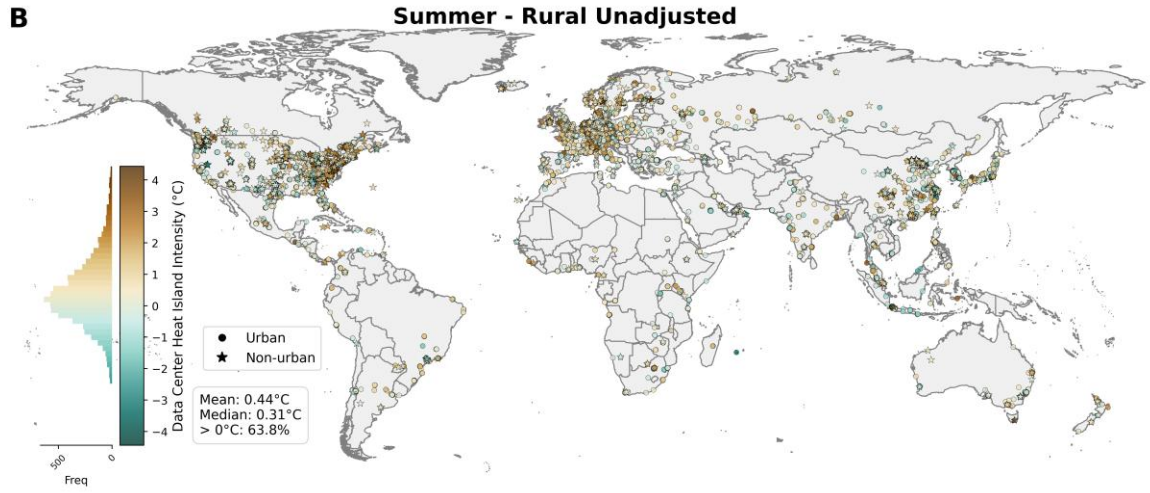

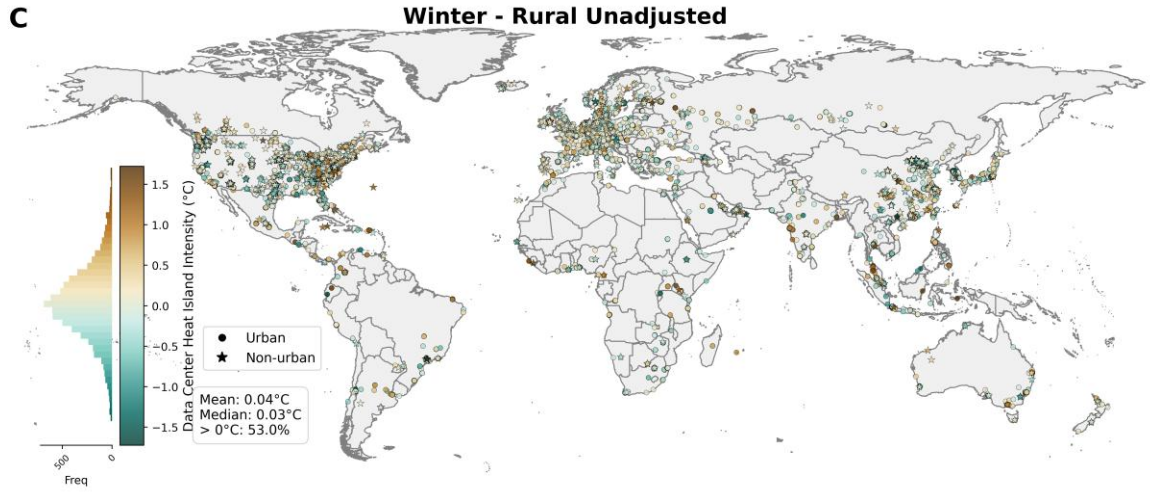

Fig. S3. Data Center Heat Island effect using the "rural unadjusted" algorithm. Distributions of the localized land surface temperature (LST) difference between the data center facility core (0–300 m radius) and its rural reference ring (300–425 m radius), representing the Data Center

600 Heat Island (DCHI) effect for (A) annual, (B) summer, and (C) winter for 2020 to 2024 using the
601 "rural unadjusted" algorithm. Positive values signify a facility that is warmer than its immediate
602 surroundings. Facilities are categorized by their presence or absence within present-day urban
603 clusters. Note that the exact locations are randomly shifted to protect proprietary data.
604

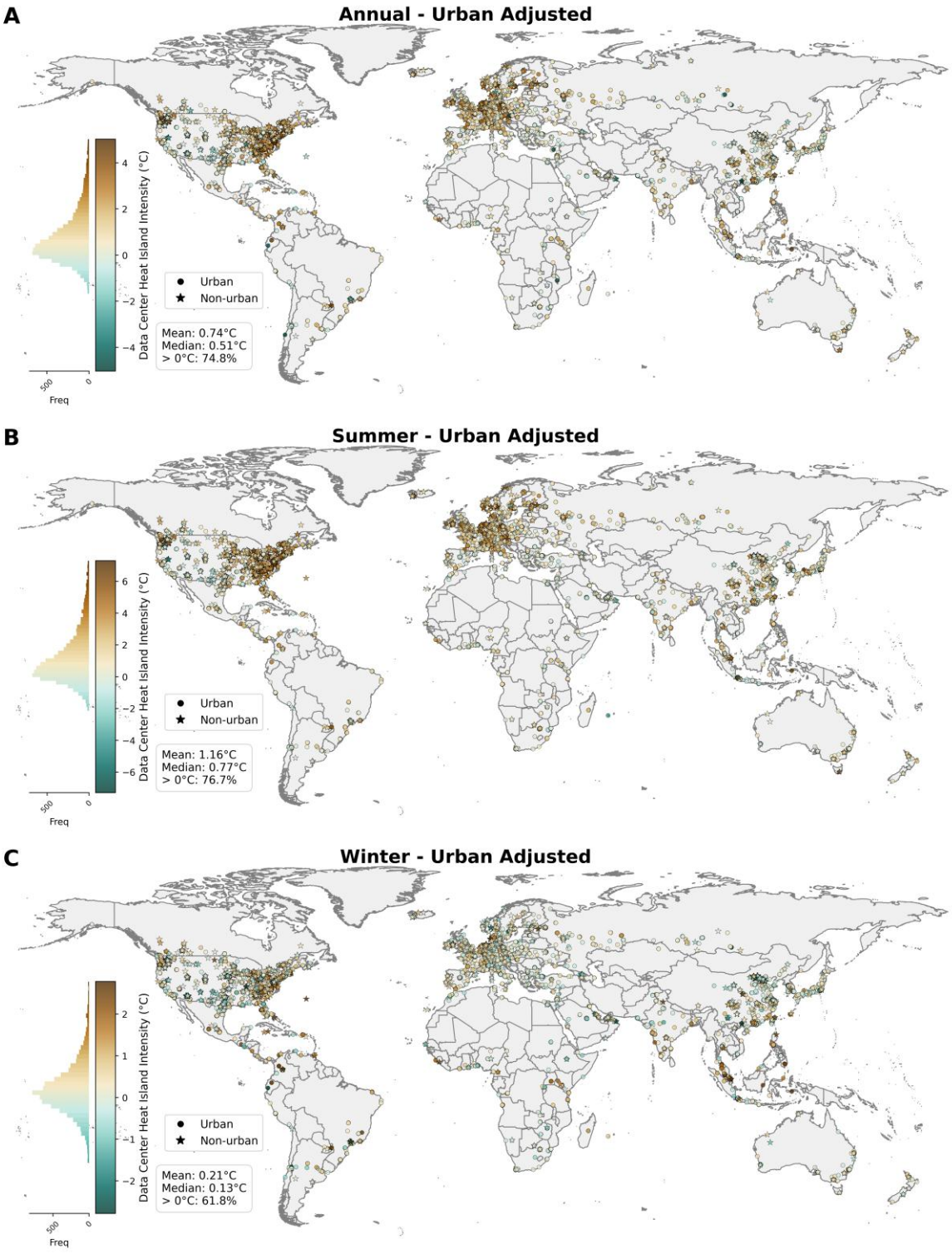

Fig. S4. Data Center Heat Island effect using the "urban adjusted" algorithm. Distributions of the localized land surface temperature (LST) difference between the data center facility core (0–300 m radius) and its rural reference ring (300–425 m radius), representing the Data Center Heat Island (DCHI) effect for (A) annual, (B) summer, and (C) winter for 2020 to 2024 using the

612 "urban adjusted" algorithm. Positive values signify a facility that is warmer than its immediate
613 surroundings. Facilities are categorized by their presence or absence within present-day urban
614 clusters. Note that the exact locations are randomly shifted to protect proprietary data.

615

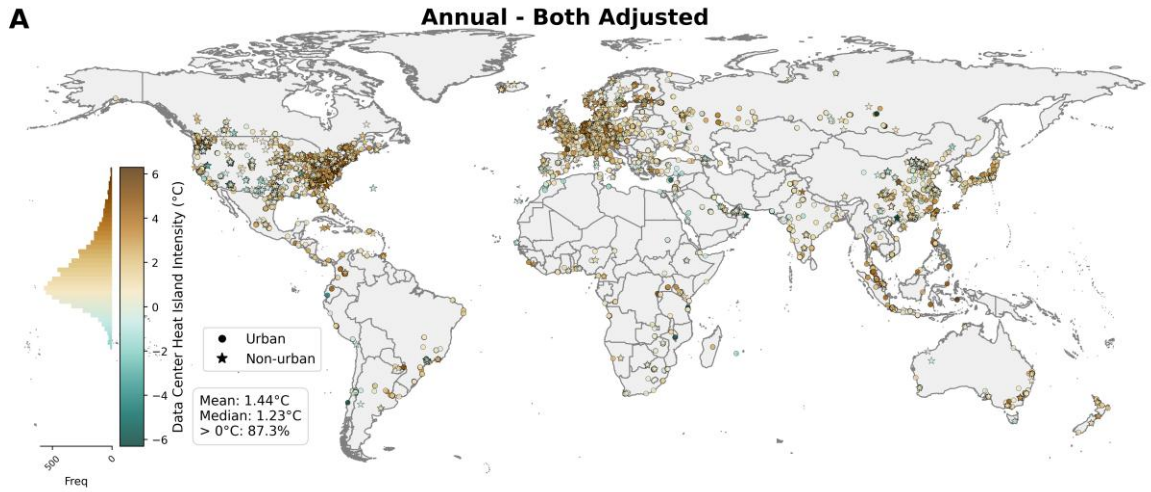

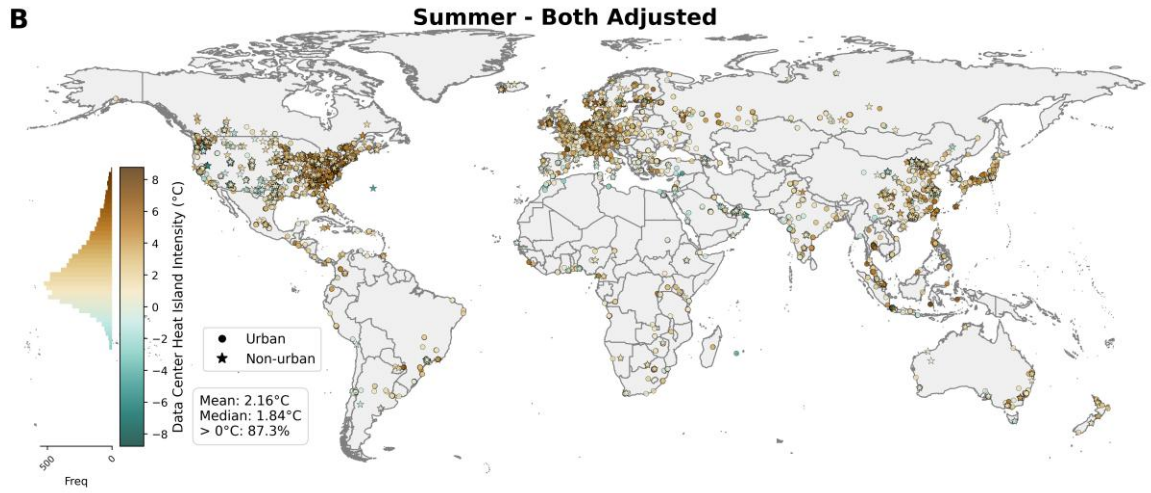

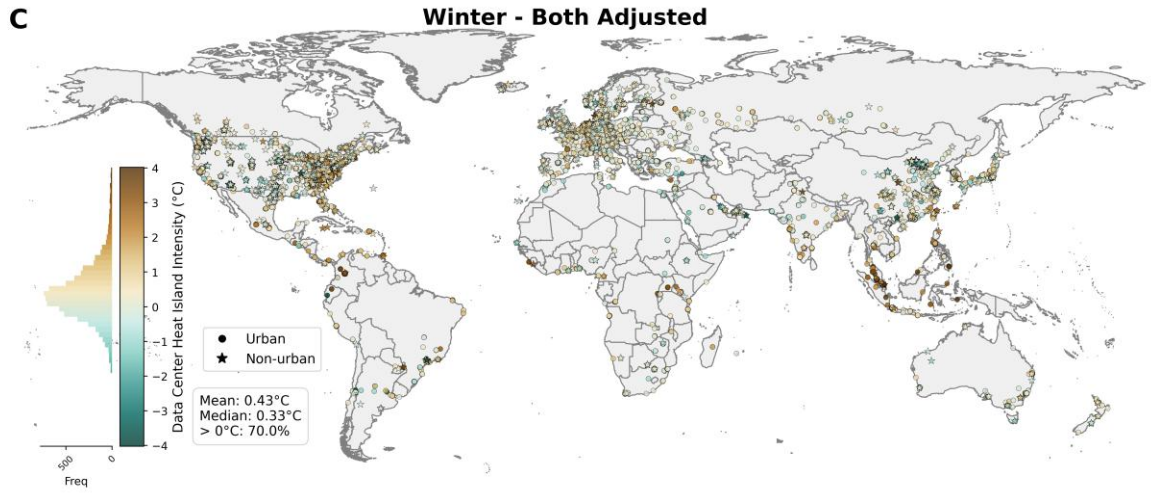

Fig. S5. Data Center Heat Island effect using the "both adjusted" algorithm. Distributions of the localized land surface temperature (LST) difference between the data center facility core (0–300 m radius) and its rural reference ring (300–425 m radius), representing the Data Center Heat

Island (DCHI) effect for (A) annual, (B) summer, and (C) winter for 2020 to 2024 using the "both adjusted" algorithm. Positive values signify a facility that is warmer than its immediate surroundings. Facilities are categorized by their presence or absence within present-day urban clusters. Note that the exact locations are randomly shifted to protect proprietary data.

627

628

629

630

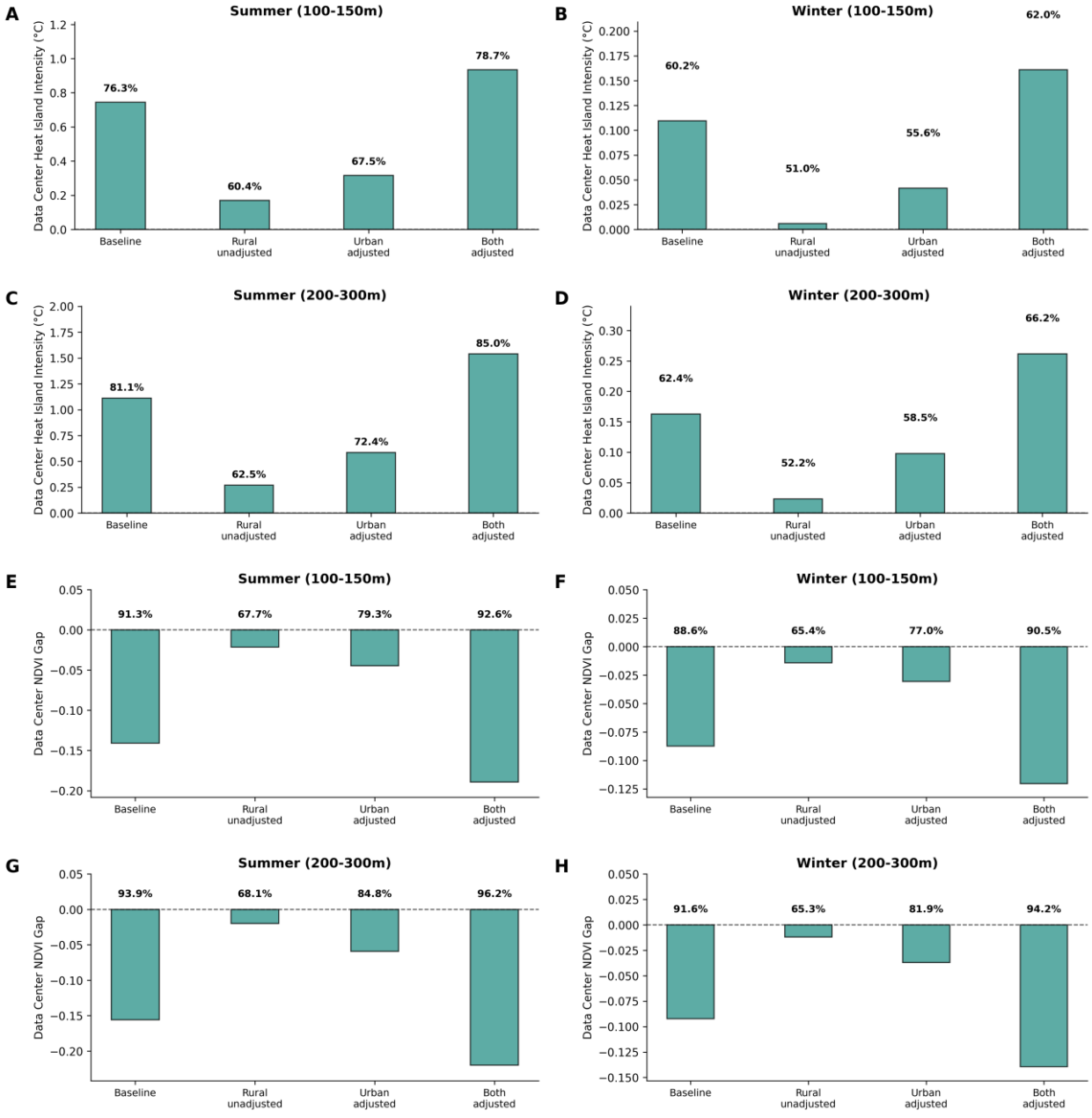

631 **Fig. S6. Sensitivity of the Data Center Heat Island and localized vegetation reduction to**
632 **smaller reference selection.** Localized land surface temperature (LST) differences (DCHI) and
633 Normalized Difference Vegetation Index (NDVI) gap between the data center facility core and
634 surrounding rural reference ring for 2020 to 2024. For DCHI, results are shown for summer and
635 winter using a (A, B) 100 m circular buffer and 100–150 m reference buffer ring and (C, D) 200
636 m circular buffer and 200–300 m reference buffer ring. Similarly, for the NDVI gap, results are
637 shown for summer and winter using a (E, F) 100 m circular buffer and 100–150 m reference buffer

ring and (G, H) 200 m circular buffer and 200–300 m reference buffer ring. Positive DCHI values signify a facility that is warmer than its immediate surroundings, while negative NDVI gap values signify a facility with less vegetation than its surroundings. The bars represent the median magnitude and the percentage of facilities with a positive DCHI or negative NDVI gap across four calculation methodologies, the standard dynamically masked and topography-controlled approach (baseline), “rural unadjusted”, “urban adjusted”, and “both adjusted”, are noted.

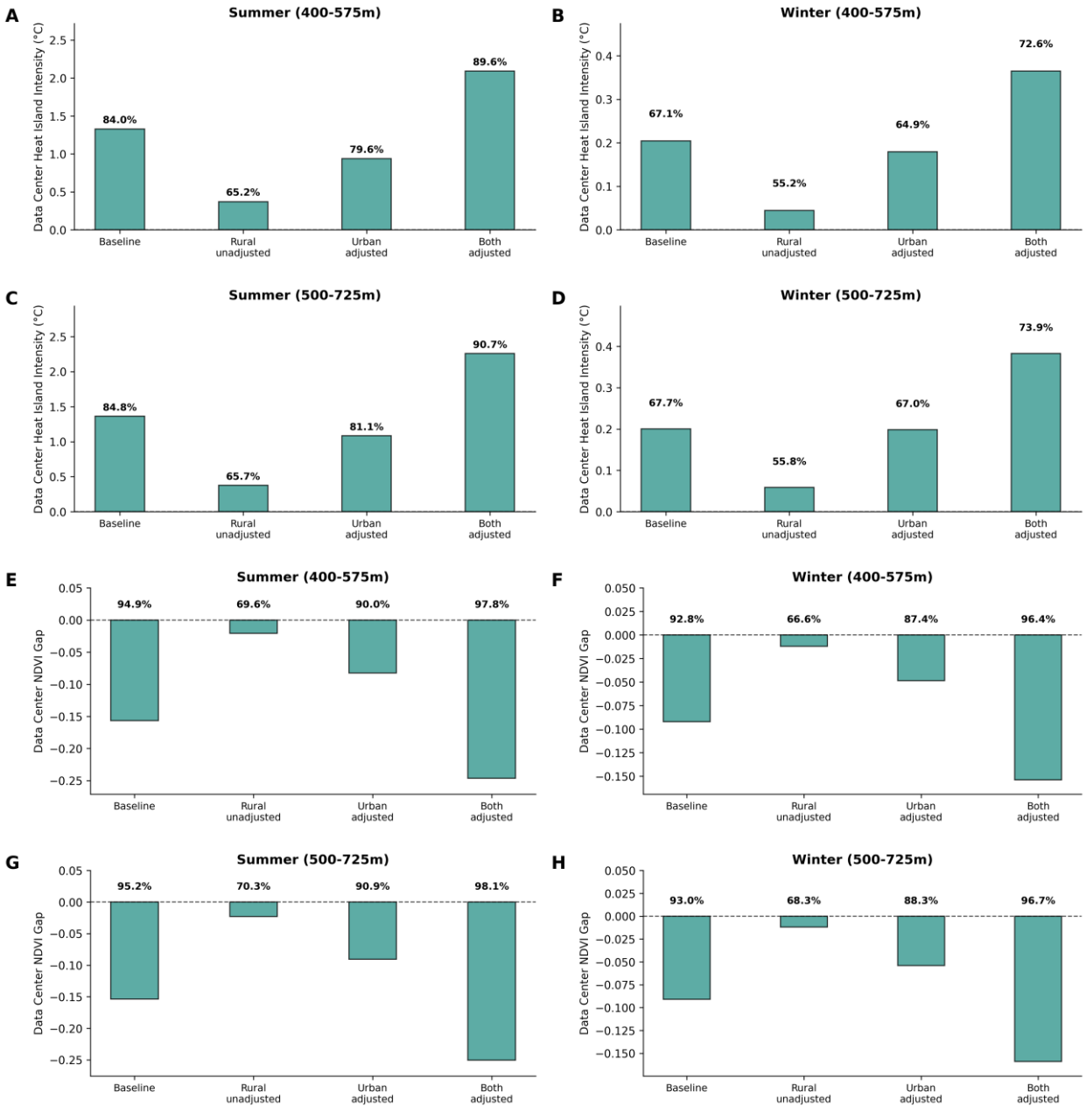

Fig. S7. Sensitivity of the Data Center Heat Island and localized vegetation reduction to larger reference selection. Localized land surface temperature (LST) differences (DCHI) and Normalized Difference Vegetation Index (NDVI) gap between the data center facility core and surrounding rural reference ring for 2020 to 2024. For DCHI, results are shown for summer and winter using a (A, B) 400 m circular buffer and 400–575 m reference buffer ring and (C, D) 500 m circular buffer and 500–725 m reference buffer ring. Similarly, for the NDVI gap, results are shown for summer and winter using a (E, F) 400 m circular buffer and 400–575 m reference buffer

ring and (G, H) 500 m circular buffer and 500–725 m reference buffer ring. Positive DCHI values signify a facility that is warmer than its immediate surroundings, while negative NDVI gap values signify a facility with less vegetation than its surroundings. The bars represent the median magnitude and the percentage of facilities with a positive DCHI or negative NDVI gap across four calculation methodologies, the standard dynamically masked and topography-controlled approach (baseline), “rural unadjusted”, “urban adjusted”, and “both adjusted”, are noted.

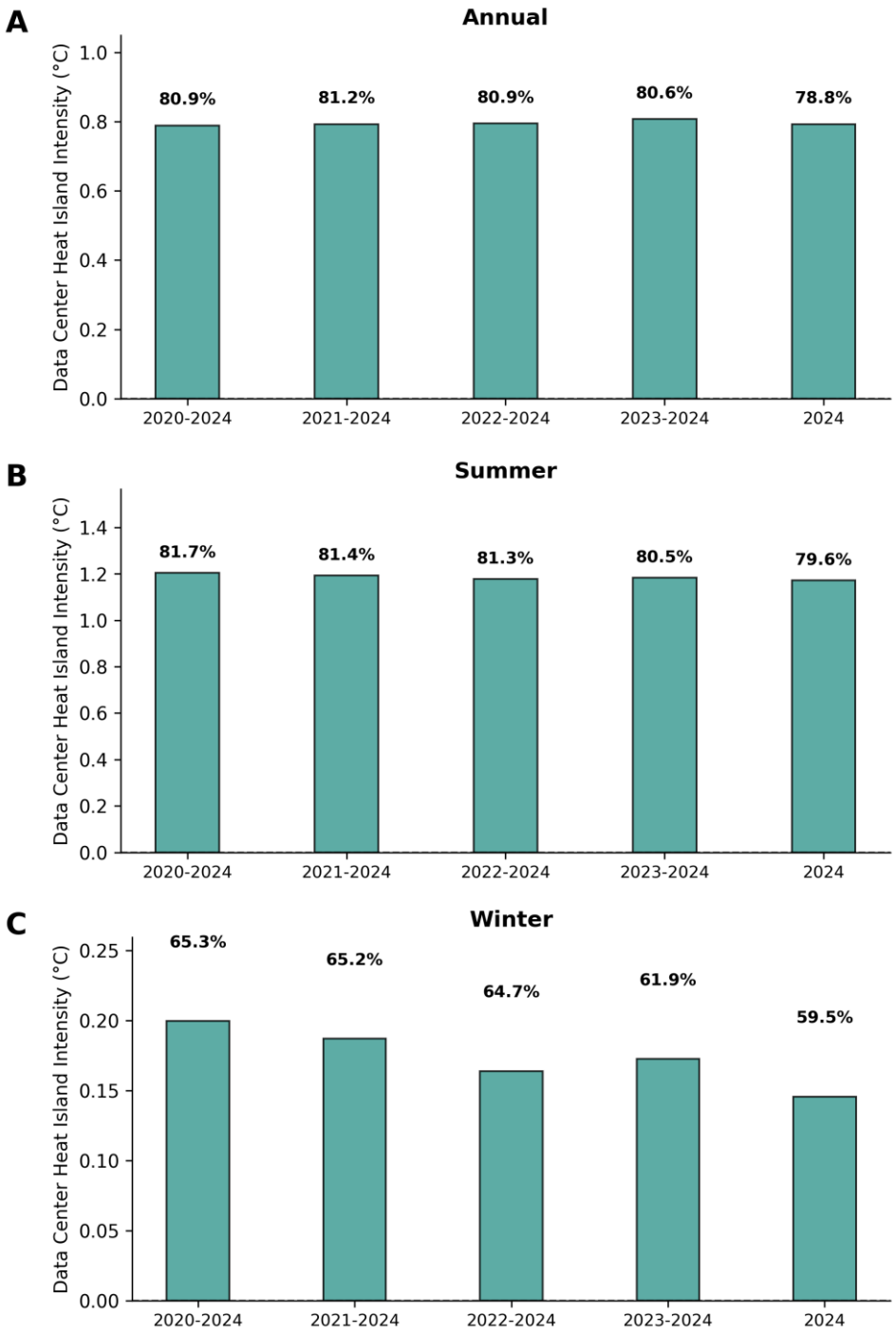

Fig. S8. Sensitivity of the Data Center Heat Island to averaging period. Localized land surface temperature (LST) differences between the data center facility core and surrounding rural reference ring, or the Data Center Heat Island (DCHI), for various averaging periods for (A) annual, (B) summer, and (C) winter. The bars represent the median magnitude and the percentage of facilities with a positive DCHI are noted.

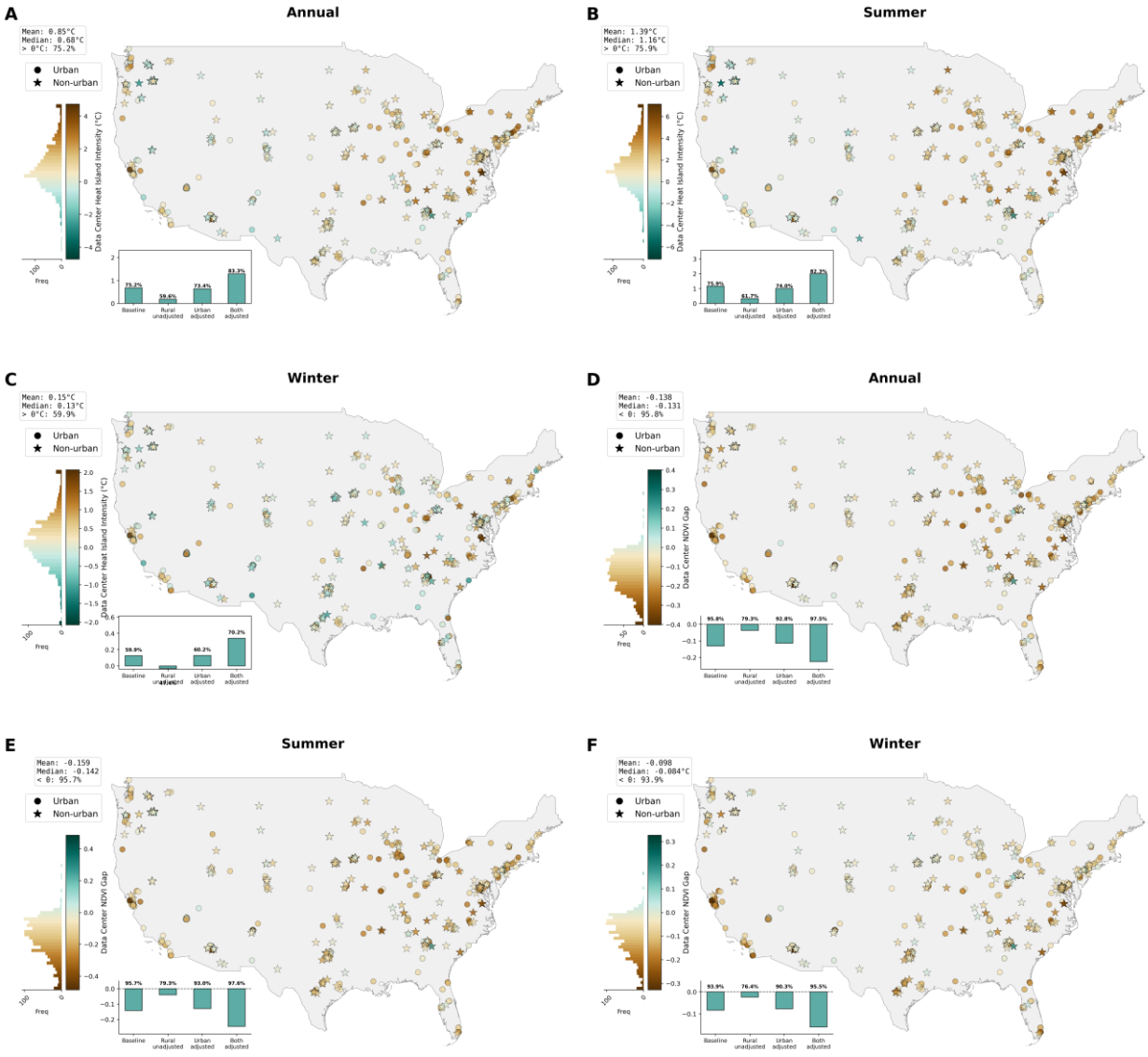

Fig. S9. Data Center Heat Island and localized vegetation reduction based on the IM3 Data Center Atlas. Distributions of the localized land surface temperature (LST) difference between the data center facility core (0–300 m radius) and the dynamically masked, topography-controlled rural reference ring (300–425 m radius), representing the Data Center Heat Island (DCHI) effect for (A) annual, (B) summer, and (C) winter for 2020 to 2024 for the United States based on the IM3 Data Center Atlas. Subfigures (D), (E), and (F) are identical, but for the Normalized Difference Vegetation Index (NDVI) gap. In both cases, facilities are categorized by their presence or absence within present-day urban clusters. The median values and percentage of positive (negative for NDVI gap) values for various algorithms are shown in the subset bar plots.

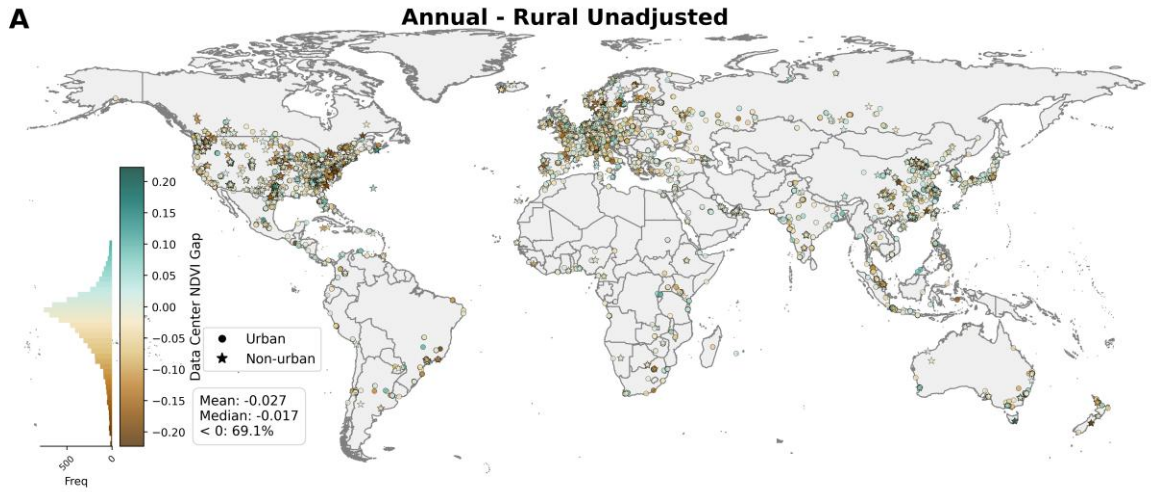

684

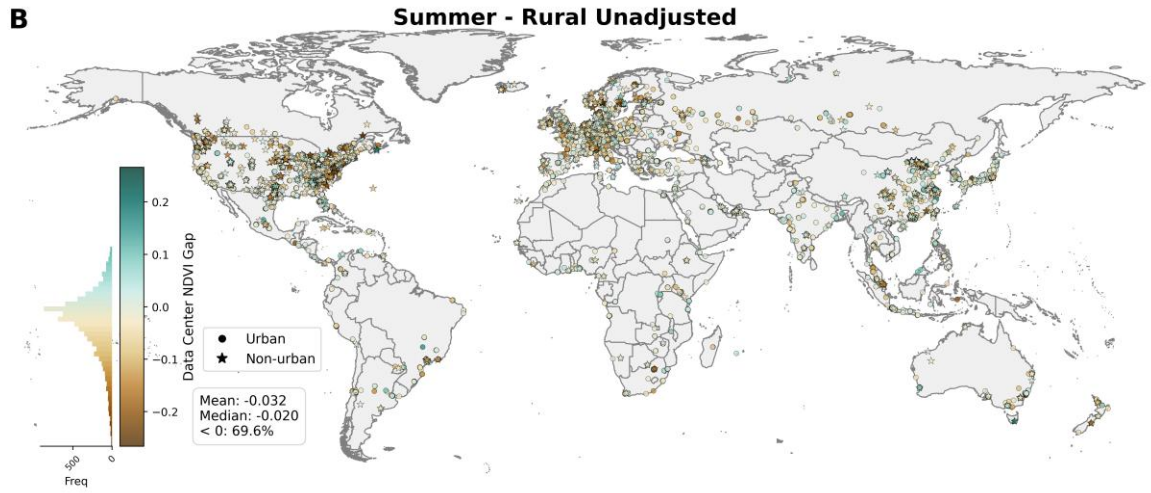

685

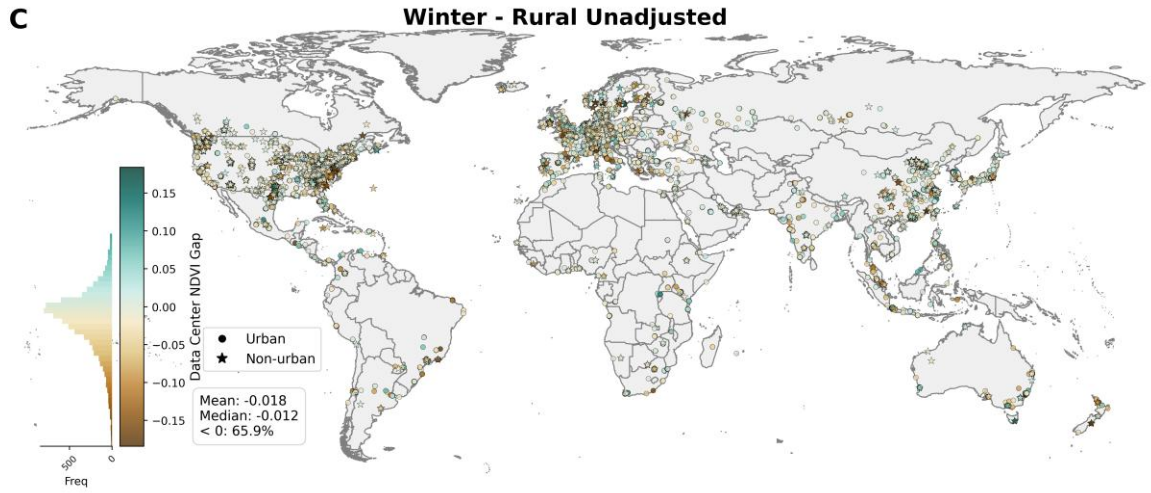

686

687 **Fig. S10. Data center-induced localized vegetation reduction using the "rural unadjusted"**
688 **algorithm.** Distributions of the localized Normalized Difference Vegetation Index (NDVI) gap
689 between the data center facility core (0–300 m radius) and its rural reference ring (300–425 m

690 radius), or the NDVI gap for (A) annual, (B) summer, and (C) winter for 2020 to 2024 using the
691 "rural unadjusted" algorithm. Positive values signify a facility that is greener than its immediate
692 surroundings. Facilities are categorized by their presence or absence within present-day urban
693 clusters. Note that the exact locations are randomly shifted to protect proprietary data.

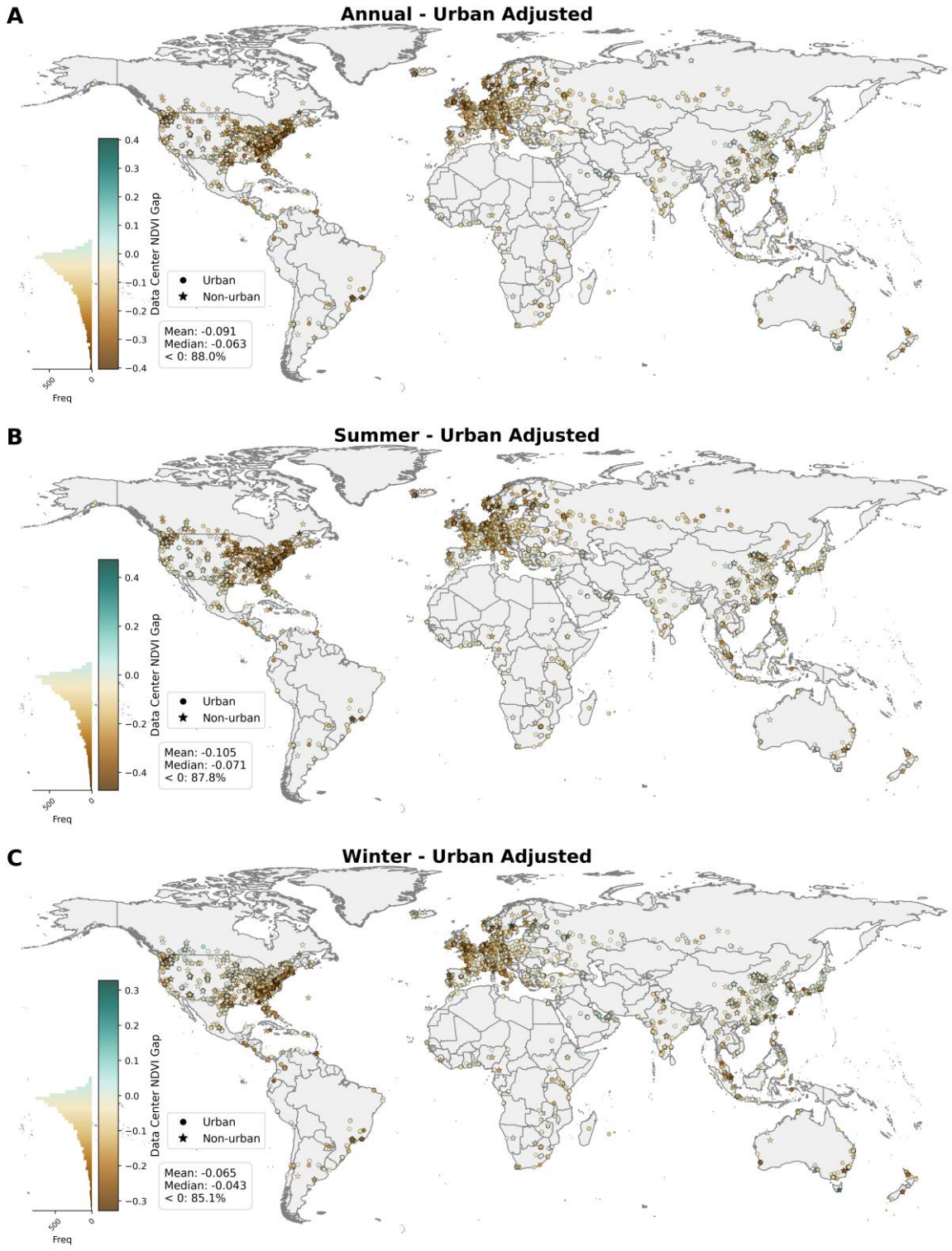

Fig. S11. Data center-induced localized vegetation reduction using the "urban adjusted" algorithm. Distributions of the localized Normalized Difference Vegetation Index (NDVI) gap between the data center facility core (0–300 m radius) and its rural reference ring (300–425 m radius), or the NDVI gap for (A) annual, (B) summer, and (C) winter for 2020 to 2024 using the

701 "urban adjusted" algorithm. Positive values signify a facility that is greener than its immediate
702 surroundings. Facilities are categorized by their presence or absence within present-day urban
703 clusters. Note that the exact locations are randomly shifted to protect proprietary data.

704

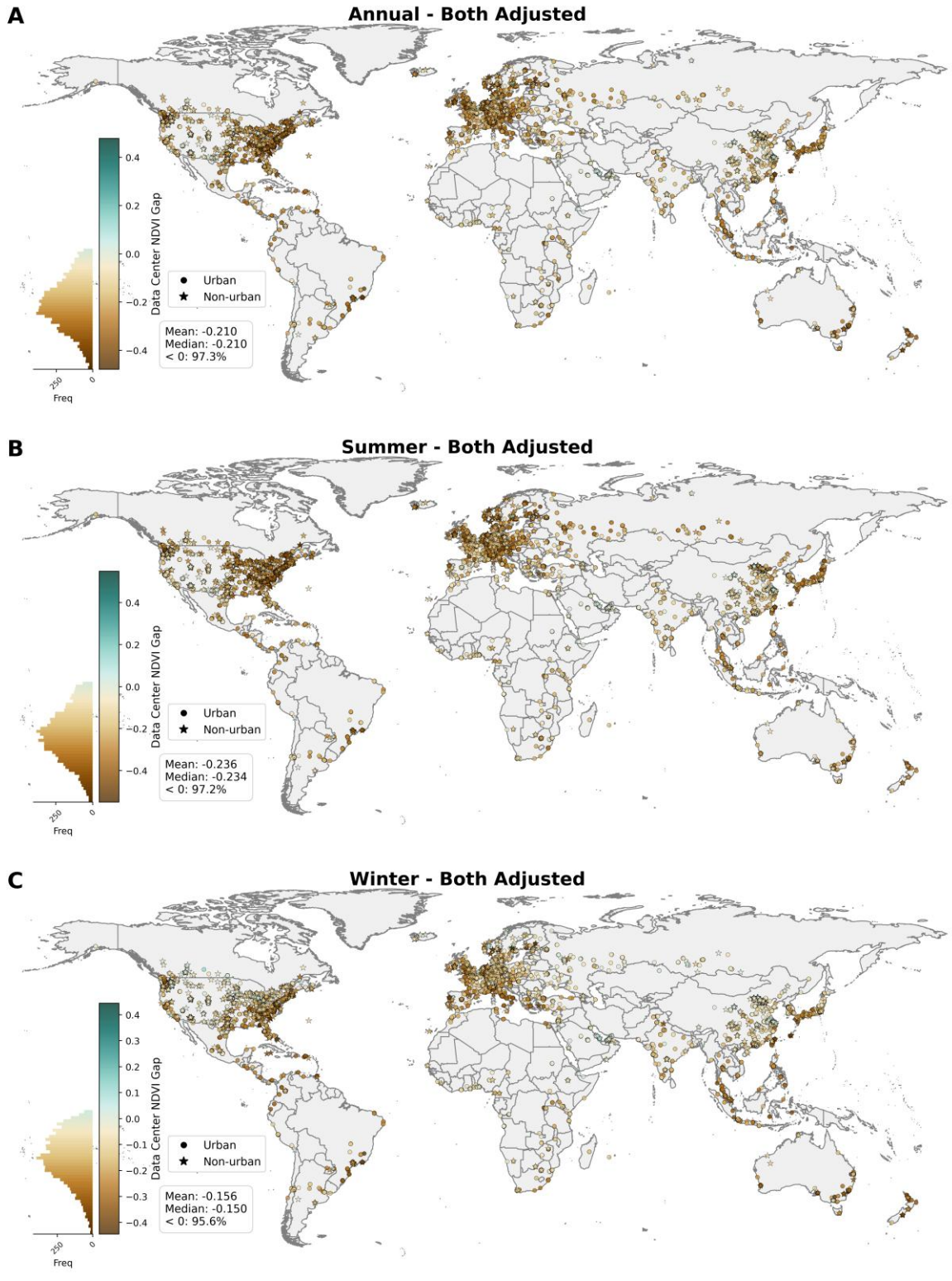

Fig. S12. Data center-induced localized vegetation reduction using the "both adjusted" algorithm. Distributions of the localized Normalized Difference Vegetation Index (NDVI) gap between the data center facility core (0–300 m radius) and its rural reference buffer (300–425 m

711 radius), or the NDVI gap for (A) annual, (B) summer, and (C) winter for 2020 to 2024 using the
712 “both adjusted” algorithm. Positive values signify a facility that is greener than its immediate
713 surroundings. Facilities are categorized by their presence or absence within present-day urban
714 clusters. Note that the exact locations are randomly shifted to protect proprietary data.

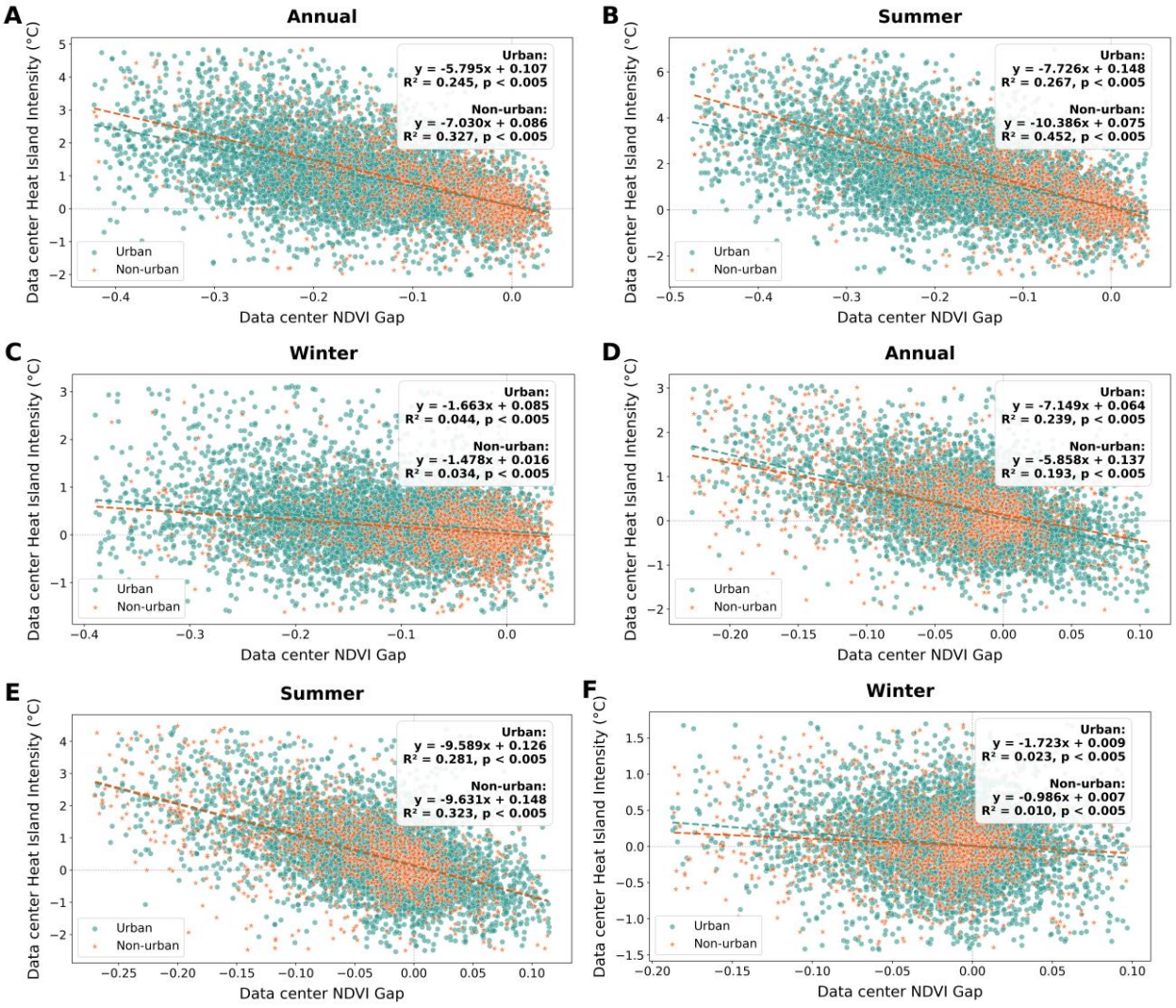

Fig. S13. Associations between data center-induced localized vegetation reduction and warming. Scatter plots demonstrating the direct spatial relationship between the local Normalized Difference Vegetation Index (NDVI) gap and Data Center Heat Island (DCHI) intensity across operational facilities for (A) annual, (B) summer, and (C) winter for the baseline algorithm. The equations for the best fit lines, the coefficient of determination (R^2), and statistical significance of the associations are shown separately for data centers inside and outside urban clusters. Subfigures (D), (E), and (F) are similar, but uses the "rural unadjusted" algorithm.

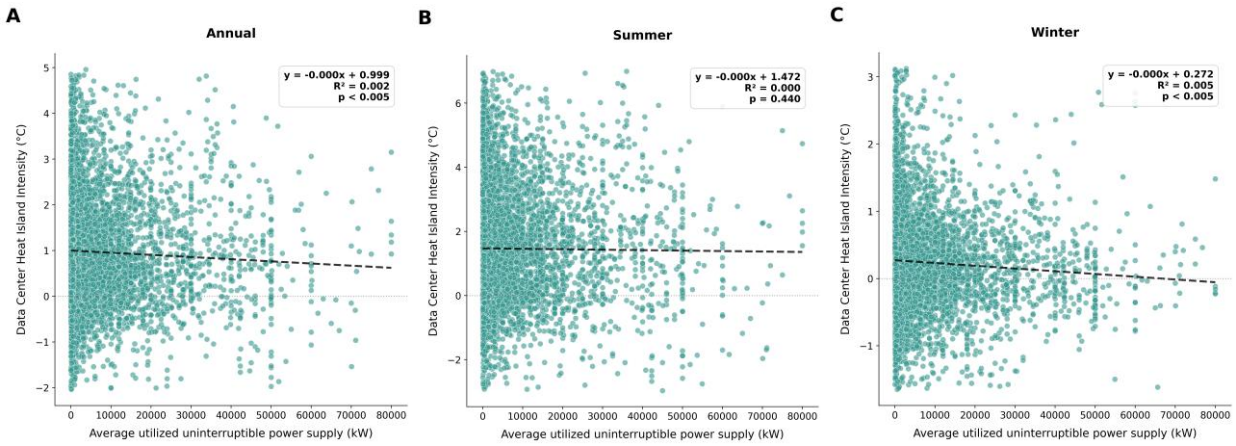

726

727 **Fig. S14. Associations between data center power supply and localized warming.** Scatter plots
728 demonstrating the direct spatial relationship between the 2020 to 2024 average utilized
729 uninterruptible data center power supply and the corresponding Data Center Heat Island (DCHI)
730 intensity across operational facilities for (A) annual, (B) summer, and (C) winter for the baseline
731 algorithm. The equations for the best fit lines, the coefficient of determination (R^2), and statistical
732 significance of the associations are shown.

733

Table S1. Local warming (Δ) of built pixels of data centers compared to their surrounding built pixels.

Time Period	Mean Δ (°C)	Median Δ (°C)	Percentage > 0 (%)
Annual	0.04	0.03	52.22
Summer	0.09	0.06	53.07
Winter	-0.01	-0.01	49.16